A&A 448, 641–653 (2006)
DOI: 10.1051/0004-6361:20054062

Astronomy & Astrophysics

Keplerian discs around post-AGB stars: a common phenomenon?⋆,⋆⋆

S. De Ruyter[1], H. Van Winckel[2], T. Maas[2,3], T. Lloyd Evans[4], L. B. F. M Waters[2,5], and H. Dejonghe[1]

[1] Sterrenkundig Observatorium, Universiteit Gent, Krijgslaan 281 S9, 9000 Gent, Belgium
e-mail: stephanie.deruyter@UGent.be
[2] Instituut voor Sterrenkunde, K.U. Leuven, Celestijnenlaan 200B, 3001 Leuven, Belgium
[3] Department of Astronomy, University of Texas, Austin, TX 78712, USA
[4] School of Physics and Astronomy, University of St. Andrews, North Haugh, St. Andrews, Fife KY16 9SS, Scotland
[5] Sterrenkundig Instituut "Anton Pannekoek", Universiteit Amsterdam, Kruislaan 403, 1098 Amsterdam, The Netherlands

Received 17 August 2005 / Accepted 6 November 2005

ABSTRACT

Aims. We aim at showing that the broad-band SED characteristics of our sample of post-AGB stars are best interpreted, assuming the circumstellar dust is stored in Keplerian rotating passive discs.
Methods. We present a homogeneous and systematic study of the Spectral Energy Distributions (SEDs) of a sample of 51 post-AGB objects. The selection criteria to define the whole sample were tuned to cover the broad-band characteristics of known binary post-AGB stars. The whole sample includes 20 dusty RV Tauri stars from the General Catalogue of Variable Stars (GCVS). We supplemented our own Geneva optical photometry with literature data to cover a broad range of fluxes from the UV to the far-IR.
Results. All the SEDs display very similar characteristics: a large IR excess with a dust excess starting near the sublimation temperature, irrespective of the effective temperature of the central star. Moreover, when available, the long wavelength fluxes show a black-body slope indicative of the presence of a component of large mm sized grains.
Conclusions. We argue that in all systems, gravitationally bound dusty discs are present. The discs must be puffed-up to cover a large opening angle for the central star and we argue that the discs have some similarity with the passive discs detected around young stellar objects. We interpret the presence of a disc to be a signature for binarity of the central object, but this will need confirmation by long-term monitoring of the radial velocities. We argue that dusty RV Tauri stars are those binaries which happen to be in the Population II instability strip.

Key words. stars: AGB and post-AGB – stars: binaries: general – stars: circumstellar matter

1. Introduction

Post-AGB stars are low and intermediate initial mass ($\leq 8-9\,M_{\odot}$) stars which have suffered a large and dusty mass-loss phase at the end of the Asymptotic Giant Branch (AGB) during which almost the whole stellar envelope was expelled. They are evolving at constant luminosity on a fast evolutionary track in which the central star crosses the HR-diagram from a cool AGB photosphere to the ionizing temperature of the central star of a Planetary Nebula (PN). Given the small evolutionary timescale of about 10^4 years, post-AGB stars are rare and not many are known (e.g. Szczerba et al. 2001; Van Winckel 2003).

Discussions on the morphology of PNe usually start with a display of the aesthetic pictures of the Hubble Space Telescope (HST) showing the complex geometry and structure of the nebulae, immediately followed by the puzzling and contradictory finding that, on the AGB, the mass-loss is found to be spherically symmetric. During the transition time, the star and circumstellar envelope must undergo fundamental and rapid changes in structure, mass-loss mode and geometry which are still badly understood. The debate on which physical mechanisms are driving the morphology changes gained even more impetus from the finding that also resolved cooler post-AGB stars or Proto-Planetary Nebulae (PPNe) display a surprisingly wide variety in shapes and structures, very early in their post-AGB evolution (Balick & Frank 2002, and references therein).

In a survey of 27 PPNe, 21 were found to be resolved (Ueta et al. 2000). Moreover, the degree of asymmetry could

⋆ Based on observations with the P7 photometer at the 0.7 m Swiss Telescope, La Silla (Chile) and at the Flemish Mercator Telescope, La Palma (Spain) and on observations with the Submillimetre Common-User Bolometer Array (SCUBA) at the James Clerk Maxwell Telescope (JCMT), Mauna Kea, Hawaii.
⋆⋆ Appendices A–C are only available in electronic form at http://www.edpsciences.org

be linked to the pole-to-equator density contrast, as determined on the basis of high spatial resolution mid-infrared images (Meixner et al. 1999). Recently also Gledhill (2005) found evidence for axi-symmetry in the dust density in his polarimetric imaging survey of candidate post-AGB stars. The detached shells correspond to stars with an optically thin expanding circumstellar envelope whereas the bipolar and unresolved targets have optically thick dust structures, probably in the form of discs. It is suggested once again that this bifurcation in morphology is rooted in the presence or absence of a binary companion, which determines whether or not a disc forms.

Stunning kinematic information resulted from the extensive CO survey of Bujarrabal et al. (2001): it appears to be a fundamental property of the omnipresent fast molecular outflow in PPNe, that it carries a huge amount of linear momentum, up to 1000 times the momentum available for a radiation driven wind. Clearly, other momentum sources have to be explored. Some molecular jets are resolved by high spatial resolution imaging (Sahai 2004). The formation process of the strongly collimated jets is, however, still badly understood. An intriguing suggestion is that the processes similar to the jet formation in low-mass young stellar objects operate and that the jets are born in accretion discs. This mechanism requires a significant amount of mass orbiting the post-AGB star. Such a disc could be present, but likely only in binary stars. Testing of such an hypothesis is severely hampered by the lack of observational information on binarity in PNe and PPNe but also on our poor theoretical understanding of AGB evolution in binary systems. Note that most objects which were detected in CO are strongly embedded and the sample is probably biased towards more massive PPNe.

Probing binarity in PNe and embedded PPNe directly with radial velocity monitoring is not easy. For optically bright post-AGB stars, this is different and some famous examples exist in which it is clear that the binary nature of the central object must have played a key role in the evolution of the system.

The most famous example is certainly HD 44179, the central star of the Red Rectangle nebula. It displays a huge and broad IR excess. The IR luminosity is 33 times stronger than the optical luminosity (Leinert & Haas 1989; Waelkens et al. 1996). Van Winckel et al. (1995) have shown that HD 44179 is a spectroscopic binary with an orbital period of 298 days. The eccentricity is a remarkably high $e = 0.37$. Since its discovery by Cohen et al. (1975), HD 44179 has often been used as an archetypical example of a C-rich post-AGB object, but it is now generally accepted that many of the remarkable phenomena and the peculiar morphology of the nebula (for an overview see Cohen et al. 2004) are closely related to the presence of a stable circumbinary disc around the binary central star. The longevity of the disc was dramatically confirmed by the detection of cool O-rich crystalline silicate dust grains in the disc (Waters et al. 1998). The mixed chemistry is best explained assuming the formation of the O-rich disc predated the more recent C-rich transition of the central object. Recent Spitzer data show, however, that also far from the central star, the nebula appears to have a dust component which is O-rich (Markwick-Kemper et al. 2005). The (chemical) history of the binary, disc and nebula is therefore far from understood. The disc is resolved in ground-based high spatial-resolution imaging at optical and near-IR wavelengths (Men'shchikov et al. 2002, and references therein) as well as in HST optical images (Cohen et al. 2004). The disc was also resolved in interferometric CO(2−1) maps, and the Keplerian kinematics of the disc were directly detected (Bujarrabal et al. 2003, 2005). HD 44179 shows a considerable amount of dust processing in the disc with indications of the presence of very large grains (Jura et al. 1997) and possibly even macro-structures (Jura & Turner 1998).

Another remarkable evolved object with a long-lived disc is HR 4049. It is a binary with an orbital period of 430 days with a remarkably high eccentricity of $e = 0.30$. Also in this object, the circumstellar material shows a mixed chemistry with both carbon rich and oxygen rich features. The SED of the dust is also very peculiar as it can be fitted with a single black-body of about 1150 K, from 1 μm down to 850 μm. These SED characteristics are very constraining and the best model for the circumstellar material is, that the dust is trapped in a very opaque dust torus at Keplerian rotation (Dominik et al. 2003). It is clear that also in this object the dusty disc plays a lead role in the (future) evolution. Other examples exist and there is substantial observational evidence that the systems are all likely surrounded by a circumstellar orbiting disc (Van Winckel 2003). Note that so far only for the Red Rectangle the Keplerian disc is spatio-kinematically resolved by CO interferometric maps (Bujarrabal et al. 2005).

To gain insight in the evolution of binary systems and their circumstellar material, we report in this contribution on a homogeneous and systematic study of a sample of objects with similar IR characteristics as the known binary post-AGB stars. The main aim is to study the broad-band SEDs in a systematic way, in order to gain insight in the possible evolutionary link between the different objects.

Our sample and the selection criteria are presented in Sect. 2. In Sect. 3 we present our photometric data complemented with the literature values and the results of the large all sky surveys. In Sect. 4 we present the detailed Spectral Energy Distribution (SED) construction of all individual objects. Distances to the objects are estimated in Sect. 5. We end this extensive study with a detailed discussion in Sect. 6. Conclusions are summarized in Sect. 7.

2. Programme stars

Our total sample of 51 stars was defined on several observational criteria inspired by the characteristics of known post-AGB stars in binary systems. The whole sample is given in Table 1. Besides these proven binaries, we discuss also RV Tauri stars with IRAS detections of good quality and a sample of newly identified objects, originally found by one of us (T. Lloyd Evans) in search of new candidate RV Tauri stars.

2.1. Confirmed binary post-AGB stars

The group of binary post-AGB stars in our sample was assembled in a rather coincidental way on the basis of independent detailed star-to-star analyses. We included the proven binaries in our programme star sample and in Col. 12 of Table 1 we

Table 1. The IRAS number, the HD number or the name from the GCVS, the spectral type, the equatorial coordinates α and δ (J2000), the effective temperature $T_{\rm eff}$, the surface gravity $\log g$, the metallicity [Fe/H], the reference for the model parameters, the type of object (post-AGB, RV Tauri or New Sample) and a reference where the orbital motion of the object can be found, are given. Note that IRAS 11472−0800 is a strongly depleted object added to our sample stars.

1	2	3	4	5	6	7	8	9	10	11	12
No	IRAS number	HD number or GCVS name	Spectral type	α (J2000) (h m s)	δ (J2000) (° ′ ″)	$T_{\rm eff}$ (K)	$\log g$ (cgs)	[Fe/H]	Reference Model Parameters	Type	Reference Binarity
1	IRAS 04166+5719	TW Cam	G3I	04 20 48.1	+57 26 26	4800	0.0	−0.5	Giridhar et al. (2000)	RV Tauri	
2	IRAS 04440+2605	RV Tau	G2I	04 47 06.8	+26 10 44	4500	0.0	−0.4	Giridhar et al. (2000)	RV Tauri	
3	IRAS 05208−2035		M0e+F	05 22 59.423	−20 32 53.03	4000	0.5	0.0	from spectral type	New Sample	
4	IRAS 06034+1354	DY Ori	G0I	06 06 12.3	+13 53 09	6000	1.5	−2.0	Gonzalez et al. (1997b)	RV Tauri	
5	IRAS 06072+0953	CT Ori	F9I	06 09 57.4	+09 52 35	5500	1.0	−2.0	Gonzalez et al. (1997a)	RV Tauri	
6	IRAS 06108+2743	SU Gem	G5I	06 14 00.8	+27 42 12	5750	1.125	−0.7	Wahlgren (1992)	RV Tauri	
7	IRAS 06160−1701	UY CMa	G0V	06 18 16.367	−17 02 34.72	5500	1.0	0.0	from spectral type	RV Tauri	
8	IRAS 06176−1036	HD 44179	F1I	06 19 58.2160	−10 38 14.691	7500	0.8	−3.3	Waelkens et al. (1992)	post-AGB	Van Winckel et al. (1995)
9	IRAS 06338+5333	HD 46703	F3I	06 37 52.4253	+53 31 01.957	6250	1.0	−1.5	from spectrum	post-AGB	Hrivnak, private communication
10	IRAS 06472−3713	ST Pup	F7I	06 48 56.4131	−37 16 33.332	5750	0.5	−1.5	Gonzalez & Wallerstein (1996)	RV Tauri	Gonzalez & Wallerstein (1996)
11	IRAS 07008+1050	HD 52961	F6I	07 03 39.6314	+10 46 13.067	6000	0.5	−4.8	Waelkens et al. (1991b)	post-AGB	Waelkens et al. (1992)
12	IRAS 07140−2321	SAO 173329	F5I	07 16 08.271	−23 27 01.61	7000	1.5	−0.8	Van Winckel (1997)	post-AGB	Van Winckel et al. (1995)
13	IRAS 07284−0940	U Mon	G0I	07 30 47.5	−09 46 37	5000	0.0	−0.8	Giridhar et al. (2000)	RV Tauri	Pollard & Cottrell (1995)
14	IRAS 08011−3627	AR Pup	F0I	08 03 01.1	−36 35 47	6000	1.5	−1.0	Gonzalez et al. (1997b)	RV Tauri	
15	IRAS 08544−4431		F3	08 56 14.182	−44 43 10.73	7250	1.5	−0.5	Maas et al. (2003)	New Sample	Maas et al. (2003)
16	IRAS 09060−2807		F5	09 08 10.1	−28 19 10	6500	1.5	−0.5	Maas et al. (2005)	New Sample	
17	IRAS 09144−4933		G0	09 16 09.1	−49 46 06	5750	0.5	−0.5	Maas et al. (2005)	New Sample	
18	IRAS 09256−6324	IW Car	F7I	09 26 53.4	−63 37 48	6700	2.0	−1.0	Giridhar et al. (1994)	RV Tauri	
19	IRAS 09400−4733		M0	09 41 52.9	−47 47 03					New Sample	
20	IRAS 09538−7622		G0	09 53 58.5	−76 36 53	5500	1.0	−0.5	Maas et al. (2005)	New Sample	
21	IRAS 10158−2844	HR 4049	A6I	10 18 07.5903	−28 59 31.201	7500	1.0	−4.5	Dominik et al. (2003)	post-AGB	Waelkens et al. (1991b)
22	IRAS 10174−5704		K:rr	10 19 18.1	−57 19 36					New Sample	
23	IRAS 10456−5712	HD 93662	K5	10 47 38.3965	−57 28 02.679	4250	0.5	0.0	from spectral type	New Sample	
24	IRAS 11000−6153	HD 95767	F0I	11 02 04.314	−62 09 42.84	7600	2.0	0.1	Van Winckel (1997)	post-AGB	Van Winckel et al. (1995)
25	IRAS 11118−5726	GK Car	M0I	11 14 01.3	−57 43 09					RV Tauri	
26	IRAS 11472−0800		F5I	11 49 48.5	−08 17 21	5750	1.0	−2.5	from spectrum		
27	IRAS 12067−4508	RU Cen	F6I	12 09 23.7	−45 25 35	6000	1.5	−2.0	Maas et al. (2002)	RV Tauri	
28	IRAS 12185−4856	SX Cen	G3V	12 21 12.6	−49 12 41	6000	1.0	−1.0	Maas et al. (2002)	RV Tauri	Maas et al. (2002)
29	IRAS 12222−4652	HD 108015	F3Ib	12 24 53.501	−47 09 07.51	7000	1.5	−0.1	Van Winckel (1997)	post-AGB	
30	IRAS 13258−8103		G5 De	13 31 07.1	−81 18 30					New Sample	
31		EN TrA	F2Ib	14 57 00.6847	−68 50 22.879	6000	1.0	−0.5	Van Winckel (1997)	RV Tauri	Van Winckel et al. (1995)
32	IRAS 15469−5311		F3	15 50 44.0	−53 20 44	7500	1.5	0.0	Maas et al. (2005)	New Sample	
33	IRAS 15556−5444		F8	15 59 32.1	−54 53 18					New Sample	
34	IRAS 16230−3410		F8	16 26 20.29	−34 17 12.3	6250	1.0	−0.5	Maas et al. (2005)	New Sample	
35	IRAS 17038−4815		G2p(R)e	17 07 36.3	−48 19 08	4750	0.5	−1.5	Maas et al. (2005)	New Sample	
36	IRAS 17233−4330		G0p(R)	17 26 57.5	−43 33 13	6250	1.5	−1.0	Maas et al. (2005)	New Sample	
37	IRAS 17243−4348	LR Sco	G2	17 27 56.1	−43 50 48	6250	0.5	0.0	Maas et al. (2005)	New Sample	
38	IRAS 17534+2603	89 Her	F3I	17 55 25.1889	+26 02 59.966	6500	1.0	0.0	Waters et al. (1993)	post-AGB	Waters et al. (1993)
39	IRAS 17530−3348	AI Sco	G4I	17 56 18.5	−33 48 47	5000	0.0	0.0	from spectrum	RV Tauri	
40	IRAS 18123+0511		G5	18 14 49.4	+05 12 55	5000	0.5	0.0	from spectral type	New Sample	
41	IRAS 18158−3445		F6	18 19 13.6	−34 44 32	6500	1.5	0.0	from spectral type	New Sample	
42	IRAS 18281+2149	AC Her	F4I	18 30 16.2	+21 52 00	5500	0.5	−1.5	Van Winckel et al. (1998)	RV Tauri	Van Winckel et al. (1998)
43	IRAS 18564−0814	AD Aql	G8I	18 59 08.1	−08 10 14	6300	1.25	−2.1	Giridhar et al. (1998)	RV Tauri	
44	IRAS 19125+0343		F2	19 15 00.8	+03 48 41	7750	1.0	−0.5	Maas et al. (2005)	New Sample	
45	IRAS 19163+2745	EP Lyr	A4I	19 18 17.5	+27 50 38	7000	2.0	−1.5	Gonzalez et al. (1997b)	RV Tauri	
46	IRAS 19157−0247		F3	19 18 22.5	−02 42 09	7750	1.0	0.0	Maas et al. (2005)	New Sample	
47	IRAS 20056+1834	QY Sge	G0 De	20 07 54.8	+18 42 57	5850	0.7	−0.4	Rao et al. (2002)	New Sample	
48	IRAS 20117+1634	R Sge	G0I	20 14 03.8	+16 43 35	5750	0.0	−0.5	Gonzalez et al. (1997b)	RV Tauri	
49	IRAS 20343+2625	V Vul	G8I	20 36 31.8	+26 36 17	5250	1.0	0.0	from spectral type	RV Tauri	
50	IRAS 22327−1731	HD 213985	A2I	22 35 27.5259	−17 15 26.889	8250	1.5	−1.0	from spectrum	post-AGB	Van Winckel et al. (1995)
51		BD+39°4926	A9I	22 46 11.2273	+40 06 26.294	7500	1.2	−2.9	Van Winckel et al. (1995)	post-AGB	Kodaira et al. (1970)

give a reference where the orbital motion of the objects was discussed. The orbital elements themselves are listed in Table B.1.

The photospheres of several binary post-AGB stars (e.g. HR 4049 (Lambert et al. 1988; Waelkens et al. 1991a), HD 44179 (Waelkens et al. 1992), HD 52961 (Van Winckel et al. 1992) and BD+39°4926 (Kodaira et al. 1970)) are strongly affected by a poorly understood selective depletion process. The basic scenario of this process is that circumstellar gas is separated from the dust and subsequently re-accreted onto the star (Mathis & Lamers 1992; Waters et al. 1992). Since that gas is devoid of refractories, the photosphere will be altered chemically, and this may result in very Fe-poor stars which are rich in non-refractories like Zn and S. This process is very efficient in the four named binaries where there is observational evidence for the presence of a dusty stable reservoir (Van Winckel et al. 1995). Efficient separation of circumstellar gas and dust is not evident and Waters et al. (1992) argued that the most favourable circumstances may occur if the circumstellar dust is indeed trapped in a stable disc. Note that for one strongly depleted object, BD+39°4926, there was no IR excess detected by IRAS.

In the few cases where ISO spectra are available, the dust processing is strong, which results in a large crystallinity fraction of the grains (e.g. Molster et al. 2002). Also the dust grain size distribution is different in discs than in outflows and where long wavelength fluxes are available, they indicate the presence of large, μm sized and even cm sized dust grains (e.g. Shenton et al. 1995).

Obviously such a disc must play an important role in these systems and, although the indirect observational evidence for the presence of a stable disc is well established in the binary stars, the actual structure let alone the formation, stability and evolution are not well understood. Note that only for HD 44179 is this disc spatially resolved. For all other objects, the presence of the disc was postulated.

2.2. Classical RV Tauri stars from the general catalogue of variable stars with strong IR excess

RV Tauri stars form a class of classical pulsating variables. They are luminous (I-II) supergiant pulsating variables, the light curve of which shows alternating deep and shallow minima with a formal period (measured between one deep minimum and the next) of 30 to 150 days and a brightness range of up to four magnitudes. The spectral type is typically F to G at minimum and G to K at maximum. There are two main photometric varieties of RV Tauri stars: the RVa types maintain a roughly constant mean brightness; RVb types show on top of their pulsational period a longer term (600 to 1500 days) periodicity.

With their high luminosity and often large IR excesses due to thermal radiation from circumstellar dust, there is general agreement that RV Tauri stars are low-mass objects in transition from the Asymptotic Giant Branch (AGB) to white dwarfs (Jura 1986). It was noted already in the seventies that many RV Tauri stars show a considerable near-IR excess caused by a hot dust component (Gehrz & Ney 1972; Gehrz 1972; Lloyd Evans 1985), which was attributed to the possible presence of a dusty disc. Morris (1987) suggested that circumstellar dust could indeed exist in a disc structure in binary systems, either in a circumbinary disc or in a disc around one of the components. The weak circumstellar CO emission (e.g. Bujarrabal et al. 1988) together with the black-body spectral index at long wavelengths observed in some RV Tauri stars (De Ruyter et al. 2005) corroborate the conclusion that the circumstellar dust is not freely expanding but confined.

In recent years it has become clear that also many RV Tauri photospheres show chemical anomalies pointing to an efficient depletion of refractory elements (Giridhar et al. 1994; Giridhar & Ferro 1995; Giridhar et al. 1998, 2000; Gonzalez et al. 1997a,b; Van Winckel et al. 1998; Maas et al. 2002). The many affected stars show that the depletion process is a very common phenomenon in evolved stars. Giridhar et al. (2005) show that depletion in RV Tauri stars is less strong when the central star is cooler, which is interpreted as pointing to a stronger dilution due to a deeper convective envelope in the cooler stars. The depletion patterns are not seen in objects for which the intrinsic metallicity is smaller than about one tenth solar ([Fe/H] ≤ -1.0).

It is clear that the observational restriction that depletion is only active in binary stars, which was formulated when only four extremely depleted objects were known, has become much less evident with the many new detections. Direct evidence for binarity, from radial velocity measurements, is difficult to obtain since RV Tauri stars have large pulsational amplitudes. Moreover, they often show the presence of shocks in the line-forming region of the photosphere making the very determination of the radial velocity difficult (e.g. Gillet et al. 1990). Nonetheless orbital elements have been determined for quite a few classical RV Tauri stars: U Mon (Pollard & Cottrell 1995), AC Her (Van Winckel et al. 1998), EN TrA (Van Winckel et al. 1999), SX Cen (Maas et al. 2002) and orbital motion is also found for IW Car (Pollard et al. 1997), EP Lyr (Gonzalez et al. 1997b) and RU Cen (Maas et al. 2002).

In this contribution we analyse the broad-band SEDs of the RV Tauri stars of the GCVS with a reliable IRAS measurement at 60 μm (e.g. Jura 1986) and compare them with the SEDs of similar objects, which are not in the Pop II Cepheid instability strip.

2.3. New sample of candidate RV Tauri stars

Lloyd Evans (1985) and Raveendran (1989) showed that the RV Tauri stars are located in a well-defined and relatively thinly-populated part of the IRAS colour–colour diagram. The defining rectangle is:

$$\begin{cases} [12]-[25] &= 1.56 + 2.5 \log [F(25)/F(12)] \\ &= 1.0 - 1.55 \\ [25]-[60] &= 1.88 + 2.5 \log [F(60)/F(25)] \\ &= 0.20 - 1.0. \end{cases} \quad (1)$$

Lloyd Evans (1997) searched for new examples of RV Tauri stars, as stars with dusty discs, in the IRAS Catalogue, and found the stars of the "new sample" discussed in this paper. The presence in this sample of stars with the infrared properties of

the GCVS sample of RV Tauri stars, but which fell outside the instability strip as judged from their spectral types and which lacked the large-amplitude RV Tauri variability, suggested that RV Tauri stars are those stars with dusty discs which are currently located within the instability strip (Lloyd Evans 1999).

Maas et al. (2005) presented a chemical abundance analysis on the basis of high signal-to-noise and high resolution spectra for 12 stars of the newly defined sample. They found that 9 stars are affected by the depletion process. In a detailed study of one object, IRAS 08544 (Maas et al. 2003); orbital elements were found which show that this star must have undergone severe binary interaction when it was an (asymptotic) giant.

In this contribution we analyse the broad-band SEDs of all 20 newly characterized stars of this sample.

2.4. Total sample

The 51 objects of our sample are presented in Table 1. In Col. 11 we differentiate between the several subtypes. Statistical studies on the occurrence and characteristics of post-AGB stars with respect to AGB stars and/or Planetary Nebulae (PNe) do not exist yet. In the most extensive catalogue description found in the literature, Szczerba et al. (2001) consider a Galactic sample of about 220 post-AGB stars known at that time. Although the overlap between the specific sample discussed here, and the total sample of Szczerba et al. (2001) is far from complete, the sample of 51 objects discussed here, forms a significant population of post-AGB stars known to date. Note that our sample was defined on the basis of a specific set of criteria explained above and our sample is not meant to cover all known evolved stars with similar SED characteristics.

3. Broad-band photometric data

In order to reconstruct the complete SEDs of our programme stars, we combined different sets of broad-band photometric data: our own Geneva optical photometry, supplemented with UV, optical, near-IR, far-IR and submillimetre photometry found in the literature.

The main difficulty in constructing the SEDs of pulsating stars with large amplitudes, like the RV Tauri objects, is the acquisition of equally phased data over a wide spectral domain. Since these data are not available, we limited our study of the broad-band energetics to the phases of minimal and maximal covered brightness.

Geneva optical photometry

We acquired Geneva optical photometry at random epochs with the 0.7 m Swiss Telescope at La Silla and with the Flemish Mercator Telescope at La Palma, using the refurbished Geneva photometer P7 (Raskin et al. 2004). Our total data set was scanned for the maximum and minimum magnitudes (see Table C.1). Observation dates, the number of measurements and the total timebases of these maxima and minima are given as well. Additional Geneva optical photometry was found in the Geneva database: the General Catalogue of Photometric Data (GCPD, `http://obswww.unige.ch/gcpd/gcpd.html`). Note these data are only given for completeness, but were not used in our analysis; except for IRAS 10456 for which the GCPD data are our only Geneva fluxes.

UBVRI photometry

UBVRI photometry for the newly-identified objects was obtained from the South African Astronomical Observatory (SAAO) service observing programme (Table C.2). This uses the 0.5 m Telescope and the 0.75 m Automatic Photometric Telescope (APT) at Sutherland. If the *UBVRI* data of the star show large variations mainly due to a large variability of the star, we plot both minima and maxima. If the number of data points available is too low or if there are no big variations, we use a mean *UBVRI*.

We also searched for Johnson and Cousins broad-band photometry in the literature and these data are given in Table C.2 as well.

Near-IR data

JHKL photometry of the newly-identified objects was obtained by T. Lloyd Evans with the 0.75 m reflector of the South African Astronomical Observatory.

These data points were complemented with near-IR data from the 2 MASS and DENIS projects and with other *JHKLM* data points from the literature (Table C.3).

Far-IR data

For the characterization of the longer wavelength part of the SEDs we use far-IR data from the IRAS Point Source Catalogue (Beichman et al. 1988, Table C.4); for some stars data from the MSX Infrared Point Source Catalogue (Egan et al. 2003) are also available (Table C.5). The IRAS satellite had four passbands, at 12, 25, 60 and 100 μm, respectively. The SPIRIT III instrument on board the MSX satellite had 6 passbands, at 4.29, 4.35, 8.3, 12.1, 14.7 and 21.3 μm.

Submillimetre data

For six stars (TW Cam, RV Tau, SU Gem, UY CMa, U Mon and AC Her) submillimetre data (see Table C.6) are available from De Ruyter et al. (2005), for HR 4049 and IRAS 20056 we use data from the other literature. For HR 4049, HD 52961 and 89 Her, we have some newly determined SCUBA 850 micron continuum measurements. The observations were carried out with the 15 m James Clerk Maxwell Telescope (JCMT) at Mauna Kea, Hawaii, during March-April 1999 (programme M99AN08). SCUBA (Holland et al. 1999) was operated in photometry mode to simultaneously obtain data at 850 μm and 450 μm. For the data reduction, the standard software SURF was used with Mars as a flux calibrator. Table 2 details the new 850 μm continuum measurements, while for 450 μm, no significant signal was detected. Note that the new 850 μm SCUBA

Table 2. New observational data at 850 μm from SCUBA.

No	Name	F_{850} (mJy)
11	HD 52961	2.8 ± 1.9
21	HR 4049	8.7 ± 2.8
38	89 Her	40.9 ± 2.4

data point for HR 4049 is, within the errors, the same as the one in Dominik et al. (2003).

For AC Her we have a flux point at 1.1 mm from Shenton et al. (1995).

Other

At the short wavelength side, we use the IUE data (International Ultraviolet Explorer, 0.115 μm–0.320 μm) from the newly extracted spectral data release (INES Archive Data Server). If there were multiple spectra available, we only considered the maximal flux.

4. Spectral energy distributions

We analyse the SEDs of our sample stars in a homogeneous and systematic way.

4.1. The stars photosphere: model parameters

The determination of the model atmospherical parameters $T_{\rm eff}$ and $\log g$, and the overall metallicity [Fe/H] is based on the analysis of high resolution spectra used in the chemical analyses of the stars. Those spectra are preferentially taken at maximum light, because of the minimal molecular veiling during the hotter phase in the light curve (Giridhar et al. 2000).

For most stars we use model parameters deduced from our own spectra (e.g. Van Winckel 1997; Maas et al. 2003, 2005), for others we use values found in the literature. For some of our sample stars (IRAS 05208, UY CMa, IRAS 10456, IRAS 18123, IRAS 18158, V Vul), however, we don't have a spectrum nor do we find any estimates for the photospheric parameters in the literature. Here we deduce the parameters on the basis of the spectral type of the star. And for some others (IRAS 09400, IRAS 10174, GK Car, IRAS 13258, IRAS 15556) we lack optical photometry. The model parameters are given in Table 1, Cols. 7 to 9. The references where we found the parameters are shown in Col. 10.

An appropriate photospheric Kurucz model – based on $T_{\rm eff}$, $\log g$ and [Fe/H] – is used for the unattenuated stellar photospheres (Kurucz 1979).

4.2. Colour excess E(B – V) determination

Light coming from a star is attenuated and reddened by material in the line-of-sight. Note that the total line-of-sight extinction is likely to contain both a circumstellar and an interstellar component.

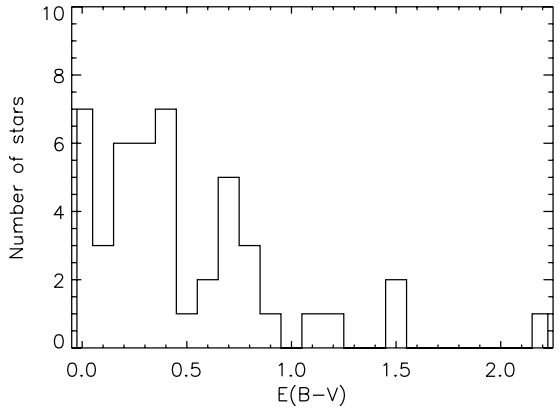

Fig. 1. The distribution of the total $E(B-V)$ found for our sample. Remark that most colour excesses are less than 1.0.

We estimate the total colour excess $E(B-V)$ by using the average interstellar extinction law given by Savage & Mathis (1979) to deredden the observed maximal UV-optical fluxes. $E(B-V)$ is found by minimizing the difference between the dereddened observed fluxes in the UV-optical, and the appropriate Kurucz model (Kurucz 1979). We scale to the J filter which is the reddest filter where no dust excess can be expected. We assume the circumstellar reddening law to be similar to the ISM law. Determining the $E(B-V)$ in this way implies that we don't correct for the contribution of the grey extinction.

Results are in Table A.1. The error on $E(B-V)$ is typically 0.1. But changing the stellar models by ±250 K in effective temperature causes a change in $E(B-V)$ of about 0.2. Thus, together with the error of 0.2 induced by the uncertainty of the temperature of the underlying photosphere, we have an uncertainty of 0.3 on the total extinction during maximal light. A distribution of the total colour excesses found for our sample stars is shown in Fig. 1. Note that the total reddening is small for most of the stars. We may thus assume that a situation with only grey extinction would be rather exceptional.

4.3. A first-order approximation: an optically thin dust fit

A broad-band SED has limited diagnostic value for constraining the chemistry and spatial distribution of the circumstellar dust. We apply an optically thin dust model as a simple first-order approximation to fit the SEDs with the prime goal to quantify the differences in SED characteristics between the different objects. We use the optically thin dust model described by Sopka et al. (1985). In this model the dust is assumed to be distributed spherically symmetric around the star from inner radius $r_{\rm in}$ to outer radius $r_{\rm out}$. Since we apply an optically thin model, the geometry of the dust is not constrained as we observe the whole volume and all dust particles contribute to the observed flux.

For more details of the model we refer to De Ruyter et al. (2005). The flux F_ν is determined by five parameters: the normalization temperature T_0, the inner radius of the dust shell $r_{\rm in}$, the outer radius of the dust shell $r_{\rm out}$, the spectral index p and the density parameter m. Applying a least square minimization

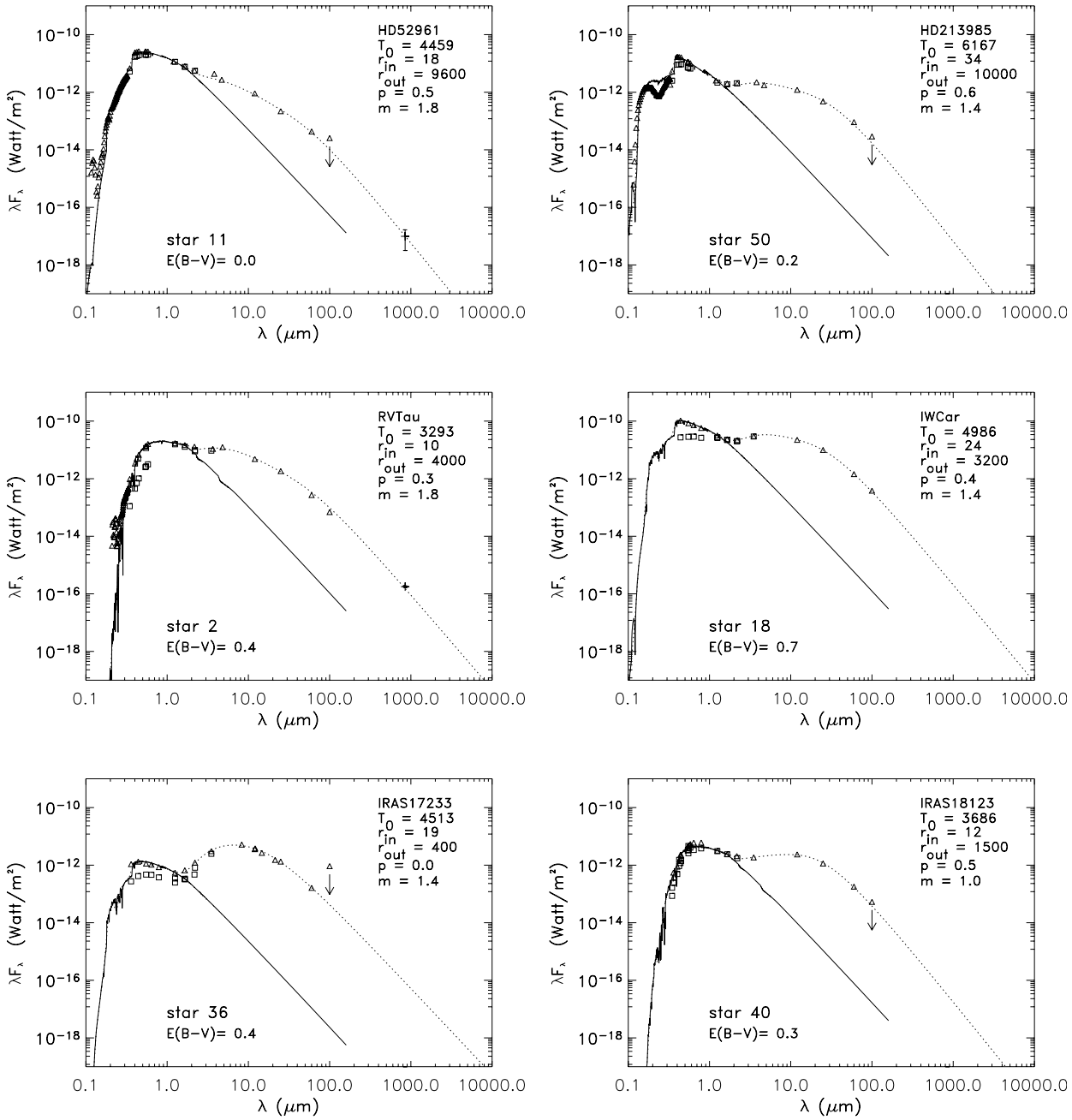

Fig. 2. The SEDs of a selection of our sample of post-AGB stars: HD 52961 and HD 213985 are examples of confirmed binary post-AGB stars, RV Tau and IW Car are genuine RV Tauri stars and IRAS 17233 and IRAS 18123 are RV Tauri like objects from the new list of T. Lloyd Evans. The dereddened fluxes are given together with the scaled photospheric Kurucz model representing the unattenuated stellar photosphere (solid line). An optically thin dust model was used to fit the IR excess (dotted line). Data found in the literature together with our 7 band Geneva photometry (only the maxima) are plotted as triangles. The minimal data points (squares) were not used for the determination of $E(B-V)$. They are shown to give an indication of the amplitude of the pulsations. Where available, crosses represent our 850 μm SCUBA data point. Error bars on the 850 μm SCUBA data point are plotted as well, for some objects though smaller than the symbols. The arrow at the 100 μm flux point signifies an upper limit.

the free parameters $r_{\rm in}$, $r_{\rm out}$, p and m are determined. Results are given in Table A.1.

4.4. SEDs

In Fig. 2 the SEDs of a selection of post-AGB stars are given. The other SEDs are given in Fig. A.1. The dereddened fluxes are plotted together with the scaled photospheric model representing the unattenuated stellar photosphere. We plotted both minimal (open triangles) and maximal (open rectangles) photometry.

HD 44179 and AR Pup are two rather exceptional stars, for which we adopted another strategy to determine the SEDs. The dust excess for HD 44179 and AR Pup starts even at shorter

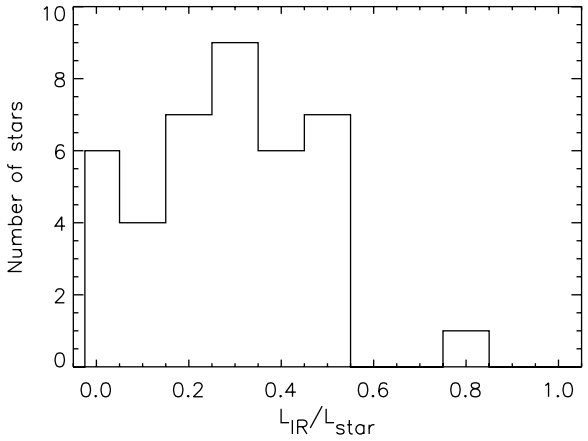

Fig. 3. The distribution of the energy conversion ratio $L_{\rm IR}/L_*$ found for our sample.

wavelengths making it impossible to scale the model photosphere to the J filter. We therefore scale to the Geneva G band data point in our least squares procedure.

The IR excess due to the presence of circumstellar dust, is in all cases very significant with BD+39°4926 a noticeable exception for which no IR excess was found. A general characteristic is that the dust energy distribution peaks at very high temperatures and that there is no evidence for large amounts of cool ($T_{\rm d} \leq 100$ K) dust: the peak of the dust SEDs lies around 10 μm and in some cases even bluer. In most cases, the dust excess starts near the dust sublimation temperature.

To determine the amount of energy reprocessed by the dust grains in the circumstellar environment, we compute the energy ratio $L_{\rm IR}/L_*$. We first calculate the stellar flux L_* by numerically integrating the scaled Kurucz model between 145 nm and 850 μm. This gives a good estimate of the unattenuated stellar flux. The energy radiated at even shorter and longer wavelengths is only a negligible fraction ($\lesssim 10^{-4}$) of the total stellar flux so we evaluate our wavelength integral boundaries as adequate. Integrating over the IR excess model described in Sect. 4.3 yields $L_{\rm IR}$. We note that the ratio $L_{\rm IR}/L_*$ (Table A.1) is high for 78% of the objects (larger than 20%). Assuming the presence of 20% grey or non-selective extinction and a mean $E(B-V)$ of 0.5, reduces $L_{\rm IR}/L_*$ with 25%, which remains, nevertheless, still large. The absorption and thermal re-radiation of the stellar radiation by the circumstellar dust is on average very efficient. In Fig. 3 the distribution of the energy conversion ratios is shown. Note that ratios larger than 1.0 (for HD 44179, AR Pup, IRAS 17233, IRAS 18158 and IRAS 20056) are omitted in the figure. Like HD 44179 (Cohen et al. 2004) and IRAS 20056 (Menzies & Whitelock 1988; Rao et al. 2002) we suspect that we only see the photosphere of those sources through scattered light. This means that we see these systems nearly edge-on.

For those stars where we have a submillimetre data point (see Table C.6) the SED follows a Rayleigh-Jeans slope from the 60−100 μm flux point redwards. Assuming that the dust emissivity at far-IR wavelengths follows a power law ($Q_\nu \sim \nu^p$), the spectral index p as determined from the slope between the 60−100 μm emission and the 850 μm flux point is close to zero. The small spectral indices in the range from 0.0 to 0.5 for most objects are consistent with the presence of a component of large grains (radius $\gtrsim 0.1$ mm) in the circumstellar environment of the stars. For those stars where we lack a submillimetre data point, the spectral index of the long wavelength slope is not well constrained.

Note that the 100 μm IRAS fluxes for some stars are affected by Galactic cirrus, so they present upper limits. In the figures an arrow is drawn. This makes it still more difficult to be sure about the slope from the 60−100 μm flux point redwards.

From all SED characteristics mentioned, we infer that the dust excess in the SEDs is clearly different from what we expect to observe in a post-AGB star where the excess represents the expanding and cooling relic of the strong AGB mass-loss episode(s).

5. Distance estimates

The typical luminosity of a lower mass post-AGB star is expected to be between 1000 and 10 000 $L_\odot$. Accurate luminosities of individual post-AGB objects are still largely unavailable since they are generally too far to obtain reliable parallaxes.

In the few cases where reliable Hipparcos parallaxes are available we have a direct probe of the distance and hence luminosity. Results are given in Table A.2. Note the large errors on the parallaxes translate in a large error box for the distance and the luminosity determinations. The parallax of HD 44179 can not be used to infer a luminosity because we know that we see only scattered light (Cohen et al. 2004). The same is probably true for AR Pup (see Sect. 4.4).

Alcock et al. (1998) reported the discovery of RV Tauri stars in the Large Magellanic Cloud (LMC). In light- and colour-curve behaviour, the classical RV Tauri stars appeared to be a direct extension of the type II Cepheids to longer periods. We use the P-L relation of Alcock et al. (1998) – derived for the LMC RV Tauri stars – to derive the luminosity for the pulsating objects in our sample. For variables with $P/2 > 12.6$ days we use

$$M_V = 2.54\,(\pm 0.48) - (3.91\,(\pm 0.36))\log(P/2)\,,\quad \sigma = 0.35. \quad (2)$$

Note that the intrinsic scatter is large, implying very significant uncertainties in the estimated absolute magnitudes of the objects. In Eq. (2) we use the fundamental period $P/2$, defined as the time between a deep and a shallow minimum. The formal period P is shown in Table A.2. We apply this extension of the period-luminosity relation known for type II Cepheids, for the RV Tauri stars from the GCVS to derive an estimate for their luminosities. Results, together with the bolometric corrections BC_V (Bessell et al. 1998) used, are listed in Table A.2. The error propagation starting from the errors in the P-L relation are given in the table as well. The objects are indeed luminous, as can be expected from post-AGB objects, but the large scatter in the P-L relation prevents more accurate luminosity estimates.

For the other objects, where we don't have a pulsation period determination, we take $L = 5000 \pm 2000\,L_\odot$. Note that it is not known whether the P-L relation of the LMC stars is directly applicable to Galactic stars. In general, the luminosities found

are smaller than, or equal to, about 5000 $L_\odot$ indicating that the population is of rather low initial mass.

By comparing the integrated fluxes of the scaled Kurucz model with the luminosity deduced from the P-L relation or the default assumed value of $L = 5000\,L_\odot$, we calculate the distance D to the star. The determined distances are shown in Table A.2. The propagated error of the poorly calibrated P-L relation, yields very uncertain luminosities and therefore also uncertain distances.

Remark that the luminosities determined by the P-L relation will not be appropriate to stars seen with the dusty disc nearly edge-on. Besides for the well-known example HD 44179, this is likely the case for AR Pup, IRAS 17233, IRAS 18158 and IRAS 20056 for which the distances listed in Table A.2 are clearly upper limits.

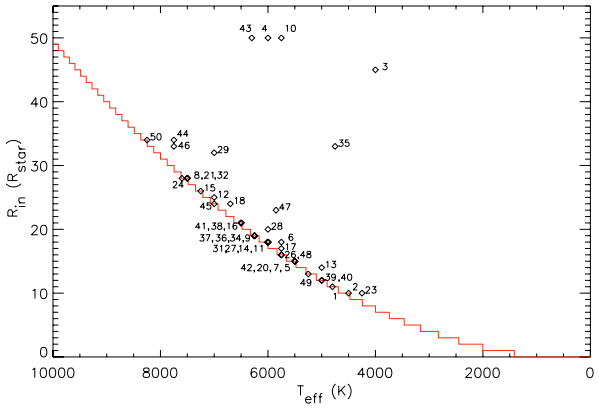

Fig. 4. The inner radii are very small. The dust must be located very close to the star: the dust excess starts for nearly all objects near the dust sublimation temperature. All SEDs show a clear near-IR excess.

6. Discussion

We presented the SEDs of all stars in our sample based on literature data supplemented with our own Geneva photometry and – where available – continuum measurements at 850 μm (Figs. 2 and A.1). Despite the different criteria for the selection of the three subsamples, it is clear that the broad-band SEDs display a high degree of uniformity. Between extremes like HR 4049 (most compact SED with a single dust temperature) and HD 44179 (largest $L_{\rm IR}/L_*$), the shape of the SEDs is very similar for all stars.

One of the most remarkable features is the start of the dust excess. In Fig. 4 we plot the inner radii of the dust components against the effective temperature for all stars and in all cases, there is dust at or very near sublimation temperature. With typical luminosity estimates, this sublimation temperature edge is at a distance smaller than about 10 AU from the central source. Moreover, the SEDs reveal that the presence of dust, very close to the object, is irrespective of the effective temperature of the central star. Note that none of the objects shows evidence for a present-day dusty mass-loss. We therefore infer that part of the dust must be gravitationally bound: any typical AGB outflow velocity would bring the dust to cooler regions within years.

Within our sample of post-AGB objects considered – confirmed binary post-AGB stars, classical RV Tauri stars and new RV Tauri-like objects – there is a wide range in the strength of the total IR excess, but the shape of the IR excess thus indicates that in all systems, the circumstellar shell is not freely expanding but stored in the system. We argue therefore that the same inner geometry as in the resolved system HD 44179 applies to the whole sample: the objects seem to be surrounded by a Keplerian disc.

From the dust modelling fit it is also clear that the outer radii are not very large either. Objects similar to the enigmatic extreme HR 4049 are UY CMa, U Mon and IRAS 17233 for which the dust temperature gradient observed is very small.
Other indirect indications for the presence of gravitionally bound dust are:

– Despite the significant IR excess, the total $E(B-V)$ for most stars is very small. Efficient redistribution of the stellar flux is clearly in contradiction with the lack of line-of-sight reddening. This implies a significant grey extinction and/or a non-spherically symmetric dust distribution. Since the objects all have a rather small total extinction, the latter is more plausible. A good independent estimate of the ISM contribution to the total extinction in the line-of-sight of all individual objects is still lacking. It must, however, be a rewarding experiment to measure those since it would help in quantifying the characteristics of the broad-band energetics of the individual objects.
– At far-IR and millimetre wavelengths, we are sampling the Rayleigh-Jeans tail of the flux distribution. The spectral index p lies, for 60% of the sample stars, in the range 0.0–0.5. The IRAS-submillimetre flux distributions are thus indicative of emission by large ($\gtrsim$0.1 mm) grains. The presence of such large grains is another indication of discs, where grain growth is facilitated. However, since we do not have submillimetre data points for all stars at our disposal, this conclusion is uncertain for those objects. Extension of the Spectral Energy Distributions (SEDs) to the submillimetre region would be helpful in constraining the disc characteristics and the grain size distribution.

Assuming the IR emission is indeed produced by an infinitely optically thick disc, we can use the ratio $L_{\rm IR}/L_*$ to estimate the opening angle θ of the disc as seen from the star. Suppose the thick disc is at a distance R from the star and at a height H above the mid-plane (total thickness of the disc is $2H$). The total inner surface of the disc is $2\pi R \times 2H$. As $L_{\rm IR}/L_*$ of the stellar energy should be absorbed by the disc, its surface must cover a solid angle of $L_{\rm IR}/L_* \times 4\pi R^2$ (Dominik et al. 2003) or

$$\tan\frac{\theta}{2} = \frac{H}{R} = \frac{L_{\rm IR}}{L_*}. \qquad (3)$$

If the disc is not optically thick, the height H would have to be even larger. If grey extinction is important for the optical fluxes, we underestimate the intrinsic stellar luminosity which has an opposite effect on the scale height. For the objects with $L_{\rm IR}/L_*$ approximately equal to 0.40, this implies $\theta \sim 44°$. Clearly, the scale height of such a disc must be significant and this disc is likely to be gas-rich. A famous example is HR 4049 for which

the energy emitted in the IR is due to the presence of a circumbinary disc with a large height ($H/R \sim 1/3$, Dominik et al. 2003).

As the material around the evolved objects is not expanding, we prefer to use the word "disc" or "gravitationally bound dust" instead of torus. Dust tori are often resolved around Proto-Planetary Nebulae, but these have very different SED characteristics since they are much colder and are probably expanding (e.g. Sánchez Contreras & Sahai 2004). Moreover, the physical sizes of the resolved tori are much larger than we expect the circumstellar material to be in the evolved objects. Recently, the very compact nature of the N band flux of the dusty environments around SX Cen and HD 52961 was directly proven by Deroo et al. (2005) thanks to the Science Demonstration Time measurements of the N band interferometric instrument (MIDI) on the VLTI. Despite the baseline of 45 m, SX Cen was not resolved which implies an upper limit of 11 mas (or 18 AU at the estimated distance of the object) at 10 μm. HD 52961 was resolved but also here, the dust emission at 10 μm comes from a very small angle of about 42 mas (~60 AU).

As argued in Sect. 4 the shape of the SEDs clearly differs from the SEDs of post-AGB stars for which dusty outflows are detected. The large optical-to-infrared energy conversion ratios indicate that the scale heights and opening angles of the discs are large. The inner rims of the discs are probably puffed up by the pressure of the hot gas in the disc.

Comparison with young stellar objects

We note that the broad-band SED characteristics, are, at first glance, very similar to the SEDs observed in young stellar objects (YSOs) in which the circumstellar passive disc is a relic of the star formation process. Despite this resemblance, differences in formation history of the discs and in the luminosity of the central stars make it likely that the characteristics will not be identical. Here we explain the similarities and differences between the structure of the post-AGB discs and the YSO discs.

Herbig Ae/Be (HAEBE) stars are the somewhat more massive analogues of the T Tauri stars, which are low-mass young stellar objects. The Spectral Energy Distributions (SEDs) of HAEBE stars are characterized by the presence of a flux excess in the infrared due to circumstellar dust and gas (Acke et al. 2004) and the geometry of this circumstellar matter is believed to be disc-like (e.g. Mannings & Sargent 1997, 2000; Fuente et al. 2003). Meeus et al. (2001) classified a sample of 14 isolated HAEBE sample stars into two groups, based on the shape of the SED. Group I contains sources in which a rising mid-IR (20−200 μm) flux excess is observed; these sources have an SED that can be fitted with a power law and a black-body continuum. Group II sources have more modest mid-IR excesses; their IR SEDs can be reconstructed by a power law only. Meeus et al. (2001) suggested that the difference between the two groups is related to the disc geometry. The irradiated passive disc models developed by Chiang & Goldreich (1997) and later extended by Dullemond et al. (2001) show that the difference in SEDs of both classes can be theoretically understood as indeed originating in the disc geometry: the mid-IR excess of the group I sources forms an indication of the flaring of the outer disc while in the group II sources, the inner rim is such that it shadows the whole disc and no flaring will occur.

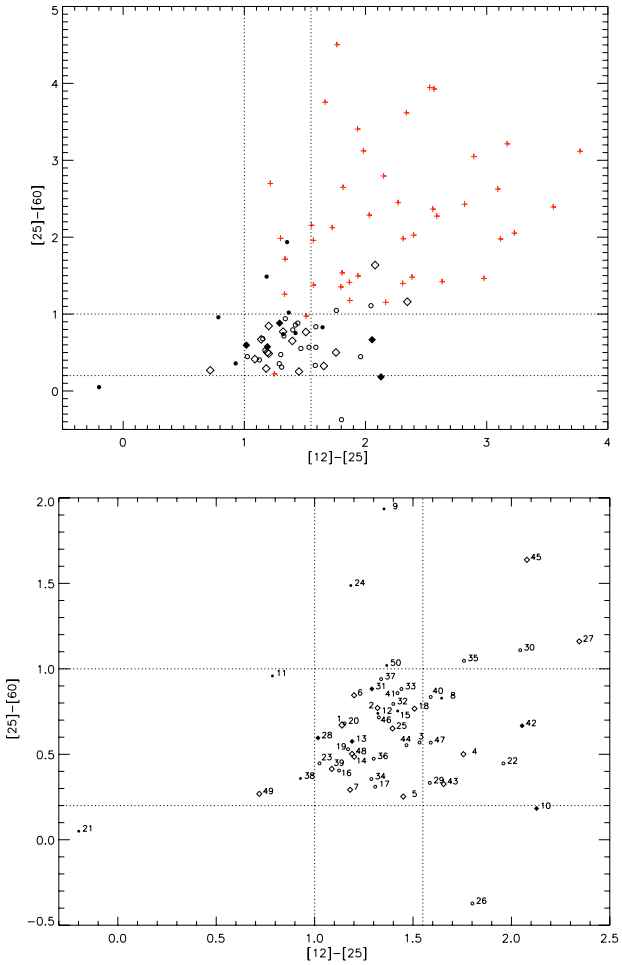

Fig. 5. *Upper-panel*: the IRAS colour–colour plot in which we mark the "RV Tauri" box as defined in Eq. (1). Note that the post-AGB objects we consider (squares and circles, filled as well as not filled) are all situated in or close to the "RV Tauri" box. The HAEBE objects (crosses) on the other hand are redder and are not in the "RV Tauri" box. *Lower-panel*: a closer view to the "RV Tauri" box. The numbers of the post-AGB objects can be found in Table 1. The classical RV Tauri stars (squares) as well as the post-AGB objects (circles) are mainly situated in the box. Note that the filled symbols are objects for which we know the orbital parameters.

To gain more insight in the differences and similarities between the stars of our sample and the young HAEBE stars, we plot the objects in a colour–colour diagram (Fig. 5) with [12] − [25] and [25] − [60] as defined in Eq. (1). Nearly all the post-AGB stars fall in the IR-box defined by T. Lloyd Evans (Sect. 2.3), while the HAEBE stars are situated on very different positions. The dust excesses of the post-AGB stars are bluer with reduced mid- and far-IR colours compared to the HAEBE stars. The post-AGB discs are therefore likely to be more compact.

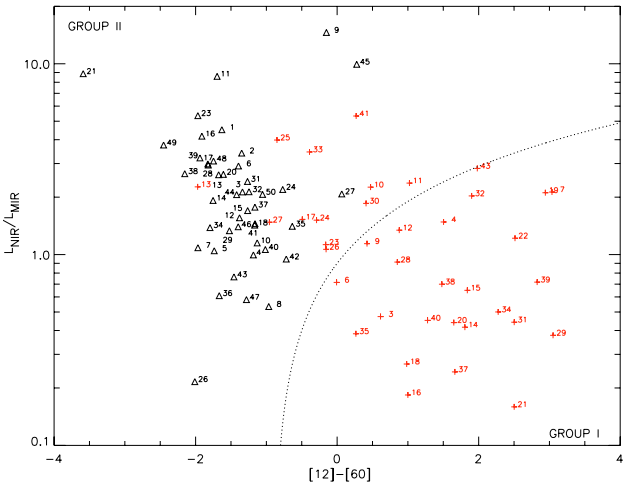

Fig. 6. Diagram based on Acke et al. (2004) and Van Boekel et al. (2003). The ratio L_{NIR}/L_{MIR} is plotted versus the non-colour corrected IRAS [12] – [60] colour. The dashed line empirically separates the group II (left) and the group I sources (right). Our sample stars are shown as triangles, the HAEBE stars as crosses. The numbers of the post-AGB objects can be found in Table 1, those of the HAEBE objects in Acke et al. (2004).

Another way of characterizing the differences between the young HAEBE stars and the old post-AGB objects can be seen in Fig. 6. The IR SED of the sample sources can be characterized by two quantities: the ratio of the near-IR luminosity L_{NIR} (derived from the broad-band J, H, K, L and M photometry) and the mid-IR luminosity L_{MIR} (the corresponding quantity based on IRAS 12, 25 and 60 μm measurements), and the non-colour corrected IRAS [12] – [60] colour. Both parameters compare the near-IR photometric data to the mid-IR IRAS measurements (Van Boekel et al. 2003; Dullemond et al. 2003). The luminosity ratio L_{NIR}/L_{MIR} represents the strength of the near-IR compared to the mid-IR excess, which is lower for group I than group II sources.

Following Van Boekel et al. (2003), we use these quantities to distinguish between group I and II in the classification of Meeus et al. (2001). We plotted all our sample stars together with the HAEBE sample stars of Acke et al. (2004) in Fig. 6. The dashed line in the diagram represents $L_{NIR}/L_{MIR} = ([12] - [60]) + 0.9$, which empirically provides the best separation between the two groups. The post-AGB stars are definitely similar to group II sources and the HAEBE group I objects are significantly redder than the post-AGB objects. Note that the IR excess of our stars starts later (near K) than that of the HAEBE stars. Given the fact that – in contrast with the HAEBE stars – for the post-AGB objects the *JHKLM* photometry is thus influenced by the stellar photosphere, we dereddened the *JHKLM* data points to make sure we don't take into account the effects of the star. To make the comparison between the HAEBE stars and the post-AGB stars more reliable, we dereddened likewise also the *JHKLM* data of the young objects. We conclude that the dust excess around our sample stars do indeed resemble the group II HAEBE sources and no indication of disc flaring is found.

The shape of the SEDs point for both the HAEBE and the post-AGB objects to a disc. Evolution, disc formation and the central stars' features, however, lead to different characteristics of the discs around both types of objects. The discs around post-AGB stars are smaller (Fig. 5) and there is little evidence for flared discs (Fig. 6).

7. Conclusions

A homogeneous and systematic study of the Spectral Energy Distributions (SEDs) of a sample of 51 post-AGB objects was presented. The selection criteria to define the sample were tuned to cover the broad-band characteristics of known binary post-AGB stars. Our whole sample included 20 dusty RV Tauri stars from the General Catalogue of Variable Stars.

We conclude that the broad-band SED characteristics of the sample are best interpreted, assuming the circumstellar dust is stored in Keplerian rotating passive discs. First-order estimates indicate that the discs are small in the radial direction and, given the large distances of these stars, they are likely only resolvable with interferometric observations.

The actual structure of those discs, let alone their formation, stability and evolution are not well understood. In Table B.1, we list the orbital elements of 15 objects of our total sample for which the orbital elements are covered in the literature. These systems are now not in contact (assuming typical post-AGB luminosities), but the orbits are all too small to accomodate a full grown AGB star. It is clear that those systems did not evolve on single star evolutionary tracks. They must have suffered a phase of strong interaction while the primary was at giant dimension. It is well known that those orbital elements are not very well understood yet, since most objects display a significant eccentricity as well (Van Winckel 2003, and references therein). One of the models argues that it is the feedback of the disc on the orbital dynamics, which will induce a large eccentricity (Artymowicz et al. 1991).

We postulate that the same formation mechanism could apply to the whole sample, which means that the objects must all be binaries. Direct detection of orbital motion and, even better, determination of the orbital elements are clearly needed but poses a non-trivial observational challenge and certainly requires a long-term project.

As our sample contains a significant fraction of all known post-AGB stars, this would lead to the conclusion that binarity and binary interaction are a widespread phenomenon among (post-) AGB stars. Dusty RV Tauri stars are those evolved binaries which happen to be in the Population II Cepheid instability strip (Lloyd Evans 1999).

Since the orbital periods detected till today, span already a wide range, from 115 to about 2600 days, we conclude that the formation of a stable orbiting disc is common and appears more and more to be a key ingredient in understanding the final evolution of a very significant fraction of binary post-AGB stars.

Acknowledgements. The staff and the service observers of the Mercator Observatory at La Palma are acknowledged for the photometric Geneva data.

This publication makes use of data products from the Two Micron All Sky Survey, which is a joint project of the University of Massachusetts and the Infrared Processing and Analysis Center/California Institute of Technology, funded by the National Aeronautics and Space Administration and the National Science Foundation.
We also made use of data from the DENIS project. This is partly funded by the European Commission through SCIENCE and Human Capital and Mobility grants. It is also supported in France by INSU, the Education Ministry and CNRS, in Germany by the Land of Baden-Würtenberg, in Spain by DGICYT, in Italy by CNR, in Austria by the Fonds zur Förderung der Wissenschaftlichen Forschung and Bundesministerium für Wissenschaft und Forschung.
This publication was also based on INES (IUE Newly Extracted Spectra) data from the IUE (International Ultraviolet Explorer) satellite.
We also like to thank S. Hony for his contribution to this paper.

References

Acke, B., van den Ancker, M. E., Dullemond, C. P., van Boekel, R., & Waters, L. B. F. M. 2004, A&A, 422, 621
Alcock, C., Allsman, R. A., Alves, D. R., et al. 1998, AJ, 115, 1921
Arellano Ferro, A. 1984, PASP, 96, 641
Artymowicz, P., Clarke, C. J., Lubow, S. H., & Pringle, J. E. 1991, ApJ, 370, L35
Balick, B., & Frank, A. 2002, ARA&A, 40, 439
Beichman, C. A., Neugebauer, G., Habing, H. J., Clegg, P. E., & Chester, T. J., ed. 1988, Infrared astronomical satellite (IRAS) catalogs and atlases, Vol. 1, Explanatory supplement
Bessell, M. S., Castelli, F., & Plez, B. 1998, A&A, 333, 231
Bujarrabal, V., Bachiller, R., Alcolea, J., & Martin-Pintado, J. 1988, A&A, 206, L17
Bujarrabal, V., Castro-Carrizo, A., Alcolea, J., & Sánchez Contreras, C. 2001, A&A, 377, 868
Bujarrabal, V., Neri, R., Alcolea, J., & Kahane, C. 2003, A&A, 409, 573
Bujarrabal, V., Castro-Carrizo, A., Alcolea, J., & Neri, R. 2005, A&A, 441, 1031
Chiang, E. I., & Goldreich, P. 1997, ApJ, 490, 368
Cohen, M., Anderson, C. M., Cowley, A., et al. 1975, ApJ, 196, 179
Cohen, M., Van Winckel, H., Bond, H. E., & Gull, T. R. 2004, AJ, 127, 2362
Dawson, D. W. 1979, ApJS, 41, 97
De Ruyter, S., Van Winckel, H., Dominik, C., Waters, L. B. F. M., & Dejonghe, H. 2005, A&A, 435, 161
Deroo, P., Van Winckel, H., Min, M., et al. 2005, A&A, submitted
Dominik, C., Dullemond, C. P., Cami, J., & van Winckel, H. 2003, A&A, 397, 595
Dullemond, C. P., Dominik, C., & Natta, A. 2001, ApJ, 560, 957
Dullemond, C. P., van den Ancker, M. E., Acke, B., & van Boekel, R. 2003, ApJ, 594, L47
Egan, M. P., Price, S. D., Kraemer, K. E., et al. 2003, VizieR Online Data Catalog, 5114, 0
Fuente, A., Rodríguez-Franco, A., Testi, L., et al. 2003, ApJ, 598, L39
Garcia-Lario, P., Manchado, A., Pych, W., & Pottasch, S. R. 1997, A&AS, 126, 479
Gehrz, R. D. 1972, ApJ, 178, 715
Gehrz, R. D., & Woolf, N. J. 1970, ApJ, 161, L213
Gehrz, R. D., & Ney, E. P. 1972, PASP, 84, 768
Gillet, D., Burki, G., & Duquennoy, A. 1990, A&A, 237, 159
Giridhar, S., & Ferro, A. A. 1995, Rev. Mex. Astron. Astrofis., 31, 23
Giridhar, S., Rao, N. K., & Lambert, D. L. 1994, ApJ, 437, 476
Giridhar, S., Lambert, D. L., & Gonzalez, G. 1998, ApJ, 509, 366
Giridhar, S., Lambert, D. L., & Gonzalez, G. 2000, ApJ, 531, 521
Giridhar, S., Lambert, D. L., Reddy, B. E., Gonzalez, G., & Yong, D. 2005, ApJ, 627, 432
Gledhill, T. M. 2005, MNRAS, 356, 883
Gledhill, T. M., Bains, I., & Yates, J. A. 2002, MNRAS, 332, L55
Goldsmith, M. J., Evans, A., Albinson, J. S., & Bode, M. F. 1987, MNRAS, 227, 143
Gonzalez, G., & Wallerstein, G. 1996, MNRAS, 280, 515
Gonzalez, G., Lambert, D. L., & Giridhar, S. 1997a, ApJ, 481, 452
Gonzalez, G., Lambert, D. L., & Giridhar, S. 1997b, ApJ, 479, 427
Holland, W. S., Robson, E. I., Gear, W. K., et al. 1999, MNRAS, 303, 659
Jura, M. 1986, ApJ, 309, 732
Jura, M., & Turner, J. 1998, Nature, 395, 144
Jura, M., Turner, J., & Balm, S. P. 1997, ApJ, 474, 741
Kilkenny, D., van Wyk, F., Marang, F., et al. 1993, South African Astron. Obs. Circ., 15, 85
Kodaira, K., Greenstein, J. L., & Oke, J. B. 1970, ApJ, 159, 485
Kurucz, R. L. 1979, ApJS, 40, 1
Lambert, D. L., Hinkle, K. H., & Luck, R. E. 1988, ApJ, 333, 917
Leinert, C., & Haas, M. 1989, A&A, 221, 110
Lloyd Evans, T. 1985, MNRAS, 217, 493
Lloyd Evans, T. 1997, Ap&SS, 251, 239
Lloyd Evans, T. L. 1999, in Asymptotic Giant Branch Stars, IAU Symp., 191, 453
Maas, T., Van Winckel, H., & Waelkens, C. 2002, A&A, 386, 504
Maas, T., Van Winckel, H., Lloyd Evans, T., et al. 2003, A&A, 405, 271
Maas, T., Van Winckel, H., & Lloyd Evans, T. 2005, A&A, 429, 297
Mannings, V., & Sargent, A. I. 1997, ApJ, 490, 792
Mannings, V., & Sargent, A. I. 2000, ApJ, 529, 391
Markwick-Kemper, F., Green, J. D., & Peeters, E. 2005, ApJ in press
Mathis, J. S., & Lamers, H. J. G. L. M. 1992, A&A, 259, L39
Meeus, G., Waters, L. B. F. M., Bouwman, J., et al. 2001, A&A, 365, 476
Meixner, M., Ueta, T., Dayal, A., et al. 1999, ApJS, 122, 221
Men'shchikov, A. B., Schertl, D., Tuthill, P. G., Weigelt, G., & Yungelson, L. R. 2002, A&A, 393, 867
Menzies, J. W., & Whitelock, P. A. 1988, MNRAS, 233, 697
Molster, F. J., Waters, L. B. F. M., Tielens, A. G. G. M., & Barlow, M. J. 2002, A&A, 382, 184
Morris, M. 1987, PASP, 99, 1115
Pollard, K. H., & Cottrell, P. L. 1995, in IAU Coll., 155, Astrophysical Applications of Stellar Pulsation, ASP Conf. Ser., 83, 409
Pollard, K. R., Cottrell, P. L., Kilmartin, P. M., & Gilmore, A. C. 1996, MNRAS, 279, 949
Pollard, K. R., Cottrell, P. L., Lawson, W. A., Albrow, M. D., & Tobin, W. 1997, MNRAS, 286, 1
Rao, N. K., Goswami, A., & Lambert, D. L. 2002, MNRAS, 334, 129
Raskin, G., Burki, G., Burnet, M., et al. 2004, in UV and Gamma-Ray Space Telescope Systems, ed. G. Hasinger, & M. J. L. Turner, Proc. SPIE, 5492, 830
Raveendran, A. V. 1989, MNRAS, 238, 945
Sánchez Contreras, C., & Sahai, R. 2004, ApJ, 602, 960
Sahai, R. 2004, in Asymmetrical Planetary Nebulae III: Winds, Structure and the Thunderbird, ASP Conf. Ser., 313, 141
Savage, B. D., & Mathis, J. S. 1979, ARA&A, 17, 73
Shenton, M., Evans, A., & Williams, P. M. 1995, MNRAS, 273, 906
Sopka, R. J., Hildebrand, R., Jaffe, D. T., et al. 1985, ApJ, 294, 242
Szczerba, R., Górny, S. K., & Zalfresso-Jundziłło, M. 2001, in Post-AGB Objects as a Phase of Stellar Evolution, 13
Ueta, T., Meixner, M., & Bobrowsky, M. 2000, ApJ, 528, 861

Van Boekel, R., Waters, L. B. F. M., Dominik, C., et al. 2003, A&A, 400, L21
Van Winckel, H. 1997, A&A, 319, 561
Van Winckel, H. 2003, ARA&A, 41, 391
Van Winckel, H., Mathis, J. S., & Waelkens, C. 1992, Nature, 356, 500
Van Winckel, H., Waelkens, C., & Waters, L. B. F. M. 1995, A&A, 293, L25
Van Winckel, H., Waelkens, C., Fernie, J. D., & Waters, L. B. F. M. 1999, A&A, 343, 202
Van Winckel, H., Waelkens, C., & Waters, L. B. F. M. 2000, in IAU Symp., 285
Van Winckel, H., Waelkens, C., Waters, L. B. F. M., et al. 1998, A&A, 336, L17
Waelkens, C., Lamers, H. J. G. L. M., Waters, L. B. F. M., et al. 1991a, A&A, 242, 433
Waelkens, C., Van Winckel, H., Bogaert, E., & Trams, N. R. 1991b, A&A, 251, 495
Waelkens, C., Van Winckel, H., Trams, N. R., & Waters, L. B. F. M. 1992, A&A, 256, L15
Waelkens, C., Van Winckel, H., Waters, L. B. F. M., & Bakker, E. J. 1996, A&A, 314, L17
Waelkens, C., & Waters, L. B. F. M. 1993, in Luminous High-Latitude Stars, ASP Conf. Ser., 45, 219
Wahlgren, G. M. 1992, AJ, 104, 1174
Waters, L. B. F. M., Cami, J., de Jong, T., et al. 1998, Nature, 391, 868
Waters, L. B. F. M., Trams, N. R., & Waelkens, C. 1992, A&A, 262, L37
Waters, L. B. F. M., Waelkens, C., Mayor, M., & Trams, N. R. 1993, A&A, 269, 242

Online Material

Appendix A: Results

Table A.1. First the estimated total colour excess $E(B-V)$ is given. Then the five parameters of the dust model are shown: the normalization temperature T_0, the inner radius of the dust shell $r_{\rm in}$, the outer radius of the dust shell $r_{\rm out}$, the spectral index p and the density parameter m. The last column lists the energy ratio $L_{\rm IR}/L_*$.

No	Name	$E(B-V)$	T_0 (K)	$r_{\rm in}$ (R_*)	$r_{\rm in}$ (AU)	$r_{\rm out}$ (R_*)	$r_{\rm out}$ (AU)	p	m	$L_{\rm IR}/L_*$
1	TW Cam	0.4 ± 0.3	3489	11	4.5 ± 1.7	5200	2100 ± 800	0.4	1.8	0.38 ± 0.05
2	RV Tau	0.4 ± 0.3	3293	10	4.7 ± 1.7	4000	1900 ± 700	0.3	1.8	0.51 ± 0.07
3	IRAS 05208	0.0 ± 0.3	2952	45	30.9 ± 7.3	1200	800 ± 200	0.6	1.4	0.06 ± 0.01
4	DY Ori	1.1 ± 0.3	4437	50	8.5 ± 2.9	1800	300 ± 100	0.4	1.2	0.12 ± 0.02
5	CT Ori	0.2 ± 0.3	4161	15	5.9 ± 2.3	3600	1400 ± 600	0.9	0.8	0.22 ± 0.03
6	SU Gem	0.8 ± 0.3	4256	18	2.9 ± 1.0	10000	1600 ± 500	0.5	1.8	0.81 ± 0.11
7	UY CMa	0.0 ± 0.3	4008	15	5.2 ± 2.0	400	100 ± 100	0.2	1.0	0.37 ± 0.05
8	HD 44179	0.0 ± 0.3	5644	28	5.5 ± 1.2	9100	1800 ± 400	0.8	1.0	14.89 ± 2.11
9	HD 46703	0.1 ± 0.3	4569	19	5.3 ± 1.1	10000	2800 ± 600	0.2	1.4	0.01 ± 0.00
10	ST Pup	0.0 ± 0.3	4307	50	3.8 ± 1.1	3300	200 ± 100	0.7	1.2	0.19 ± 0.03
11	HD 52961	0.0 ± 0.3	4459	18	5.5 ± 1.2	9600	2900 ± 600	0.5	1.8	0.11 ± 0.02
12	SAO 173329	0.4 ± 0.3	5215	25	5.6 ± 1.2	4400	1000 ± 200	0.6	1.2	0.24 ± 0.03
13	U Mon	0.0 ± 0.3	3625	14	5.3 ± 2.0	400	200 ± 100	0.1	1.2	0.12 ± 0.02
14	AR Pup	0.6 ± 0.3	4534	18	3.6 ± 1.3	6300	1300 ± 400	0.9	1.4	4.04 ± 0.57
15	IRAS 08544	1.5 ± 0.3	5434	26	5.4 ± 1.1	8300	1700 ± 400	0.8	1.2	0.31 ± 0.04
16	IRAS 09060	0.8 ± 0.3	4878	21	5.5 ± 1.2	8900	2300 ± 500	0.8	1.6	0.43 ± 0.06
17	IRAS 09144	2.2 ± 0.3	4307	17	5.6 ± 1.2	4600	1500 ± 300	0.8	1.4	0.44 ± 0.06
18	IW Car	0.7 ± 0.3	4986	24	3.5 ± 1.2	3200	500 ± 200	0.4	1.4	0.41 ± 0.06
19	IRAS 09400									
20	IRAS 09538	0.4 ± 0.3	4032	15	5.4 ± 1.2	2700	1000 ± 200	0.3	1.8	0.53 ± 0.07
21	HR 4049	0.2 ± 0.3	5541	28	5.5 ± 1.2	100	20 ± 4	0.4	1.8	0.31 ± 0.04
22	IRAS 10174									
23	IRAS 10456	0.3 ± 0.3	3149	10	6.1 ± 1.4	1800	1100 ± 300	0.7	1.6	0.36 ± 0.05
24	HD 95767	0.7 ± 0.3	5519	28	5.3 ± 1.1	10000	1900 ± 400	0.4	1.6	0.29 ± 0.04
25	GK Car									
26	IRAS 11472	0.4 ± 0.3	4357	16	5.3 ± 1.2	1800	600 ± 100	0.9	0.0	0.41 ± 0.06
27	RU Cen	0.3 ± 0.3	4529	18	3.2 ± 1.1	7900	1400 ± 500	0.8	0.6	0.03 ± 0.00
28	SX Cen	0.3 ± 0.3	4452	20	2.1 ± 0.7	3000	300 ± 100	0.5	1.6	0.29 ± 0.04
29	HD 108015	0.2 ± 0.3	5248	32	7.2 ± 1.5	7500	1700 ± 400	0.9	1.2	0.57 ± 0.08
30	IRAS 13258									
31	EN TrA	0.3 ± 0.3	4424	18	2.1 ± 0.7	4000	500 ± 100	0.4	1.6	0.38 ± 0.05
32	IRAS 15469	1.5 ± 0.3	5499	28	5.5 ± 1.2	8500	1700 ± 300	0.3	1.8	0.58 ± 0.08
33	IRAS 15556									
34	IRAS 16230	0.7 ± 0.3	4651	19	5.3 ± 1.1	1800	500 ± 100	0.6	1.0	0.26 ± 0.04
35	IRAS 17038	0.2 ± 0.3	3492	33	16.0 ± 3.6	10000	4900 ± 1100	0.4	1.8	0.28 ± 0.04
36	IRAS 17233	0.4 ± 0.3	4513	19	5.3 ± 1.1	400	100 ± 0	0.0	1.4	3.14 ± 0.44
37	IRAS 17243	0.7 ± 0.3	4581	19	5.3 ± 1.1	3800	1100 ± 200	0.3	1.6	0.50 ± 0.07
38	89 Her	0.0 ± 0.3	4785	21	3.3 ± 1.1	2400	400 ± 100	0.4	1.8	0.58 ± 0.08
39	AI Sco	0.3 ± 0.3	3657	12	3.7 ± 1.3	1000	300 ± 100	0.3	1.8	0.50 ± 0.07
40	IRAS 18123	0.3 ± 0.3	3686	12	5.3 ± 1.2	1500	700 ± 100	0.5	1.0	0.39 ± 0.06
41	IRAS 18158	0.9 ± 0.3	4824	21	5.5 ± 1.2	7000	1800 ± 400	0.6	1.4	1.04 ± 0.15
42	AC Her	0.1 ± 0.3	4036	15	3.7 ± 1.3	900	200 ± 100	0.3	0.2	0.04 ± 0.01
43	AD Aql	0.6 ± 0.3	4691	50	8.0 ± 2.8	2000	300 ± 100	0.7	0.0	0.03 ± 0.00
44	IRAS 19125	1.2 ± 0.3	5748	34	6.2 ± 1.3	7700	1400 ± 300	0.5	1.6	0.45 ± 0.06
45	EP Lyr	0.5 ± 0.3	5143	24	3.7 ± 1.3	10000	1500 ± 500	0.3	1.2	0.01 ± 0.00
46	IRAS 19157	0.8 ± 0.3	5740	33	6.0 ± 1.3	5600	1000 ± 200	0.5	1.4	0.44 ± 0.06
47	IRAS 20056	0.7 ± 0.3	4216	23	7.4 ± 1.6	1400	400 ± 100	0.3	1.4	3.16 ± 0.45
48	R Sge	0.4 ± 0.3	4236	16	3.4 ± 1.2	1800	400 ± 100	0.4	1.6	0.31 ± 0.04
49	V Vul	0.1 ± 0.3	3902	13	3.7 ± 1.3	1400	400 ± 100	0.7	1.4	0.31 ± 0.04
50	HD 213985	0.2 ± 0.3	6167	34	5.5 ± 1.1	10000	1600 ± 300	0.6	1.4	0.24 ± 0.03
51	BD+39°4926	0.2 ± 0.3								

Table A.2. For those stars for which we have a parallax obtained by Hipparcos, we derive the distance D (pc) and the luminosity L ($10^3\,L_\odot$) based on that parallax. In the second part of the table, distance and luminosity estimates are given based on the P-L relation of Alcock et al. (1998). Periods P (days) are from SIMBAD and bolometric corrections BC_V from Bessell et al. (1998). The luminosity L (in $10^3\,L_\odot$) and the distance D (in kpc) are given together with the estimated errors. Where we don't have a pulsation period, distances are estimated based on a luminosity of $L = 5000 \pm 2000\,L_\odot$.

No	Name	Parallax (mas)	Distance D (pc)	L ($10^3\,L_\odot$)	Period P (days)	BC_V	L ($10^3\,L_\odot$)	Distance D (kpc)
1	TW Cam				85.6	−0.36	3.8 ± 2.6	2.8 ± 1.0
2	RV Tau				78.698	−0.51	3.8 ± 2.6	2.1 ± 0.7
3	IRAS 05208					−0.98		4.1 ± 0.8
4	DY Ori				60.26	0.00	1.6 ± 1.0	1.9 ± 0.6
5	CT Ori				135.52	−0.08	6.0 ± 4.5	6.6 ± 2.5
6	SU Gem				50.12	−0.03	1.2 ± 0.8	2.2 ± 0.7
7	UY CMa				113.9	−0.08	4.5 ± 3.3	8.5 ± 3.1
8	HD 44179	2.62 ± 2.37	200–382–4000	0.01–0.03–3.81		0.11		<4.6
9	HD 46703					0.06		4.3 ± 0.9
10	ST Pup				18.8864	−0.01	0.3 ± 0.1	1.3 ± 0.4
11	HD 52961					0.04		2.3 ± 0.5
12	SAO 173329					0.11		7.0 ± 1.5
13	U Mon	1.45 ± 0.82	441–690–1587	1.21–2.96–15.65	92.26	−0.24	3.8 ± 2.7	0.8 ± 0.3
14	AR Pup	2.75 ± 1.16	256–364–629	0.03–0.06–0.17	75	0.00	2.2 ± 1.5	<1.8
15	IRAS 08544					0.11		0.8 ± 0.2
16	IRAS 09060					0.08		4.4 ± 0.9
17	IRAS 09144					−0.01		2.7 ± 0.6
18	IW Car				67.5	0.08	1.7 ± 1.2	0.7 ± 0.2
19	IRAS 09400							
20	IRAS 09538					−0.08		7.7 ± 1.6
21	HR 4049	1.50 ± 0.63	469–667–1149	1.67–3.39–10.05		0.11		0.8 ± 0.2
22	IRAS 10174							
23	IRAS 10456	1.18 ± 0.60	562–847–1724	3.31–7.52–31.15		−0.70		0.7 ± 0.1
24	HD 95767					0.10		2.0 ± 0.4
25	GK Car				55.6			
26	IRAS 11472					−0.03		9.7 ± 2.0
27	RU Cen				64.727	0.00	1.7 ± 1.2	1.6 ± 0.6
28	SX Cen				32.8642	0.02	0.6 ± 0.4	1.3 ± 0.4
29	HD 108015					0.11		2.5 ± 0.5
30	IRAS 13258							
31	EN TrA				36.9	0.02	0.7 ± 0.4	1.1 ± 0.3
32	IRAS 15469					0.11		1.6 ± 0.3
33	IRAS 15556							
34	IRAS 16230					0.06		6.0 ± 1.2
35	IRAS 17038					−0.36		4.6 ± 1.0
36	IRAS 17233					0.05		<9.4
37	IRAS 17243					0.07		3.9 ± 0.8
38	89 Her	1.02 ± 0.59	621–980–2326	1.38–3.45–19.43	70	0.09	1.8 ± 1.2	0.7 ± 0.2
39	AI Sco				71.0	−0.24	2.5 ± 1.7	1.9 ± 0.7
40	IRAS 18123					−0.24		5.2 ± 1.1
41	IRAS 18158					0.08		<10.3
42	AC Her				75.4619	−0.07	2.4 ± 1.6	1.3 ± 0.4
43	AD Aql				65.4	0.06	1.7 ± 1.1	4.5 ± 1.5
44	IRAS 19125					0.09		1.9 ± 0.4
45	EP Lyr				83.315	0.11	2.3 ± 1.6	3.2 ± 1.1
46	IRAS 19157					0.09		4.2 ± 0.9
47	IRAS 20056					−0.03		<9.8
48	R Sge				70.594	0.00	2.0 ± 1.4	1.8 ± 0.6
49	V Vul				75.72	−0.15	2.6 ± 1.8	2.0 ± 0.7
50	HD 213985					0.04		3.6 ± 0.7
51	BD+39°4926					0.11		4.8 ± 1.0

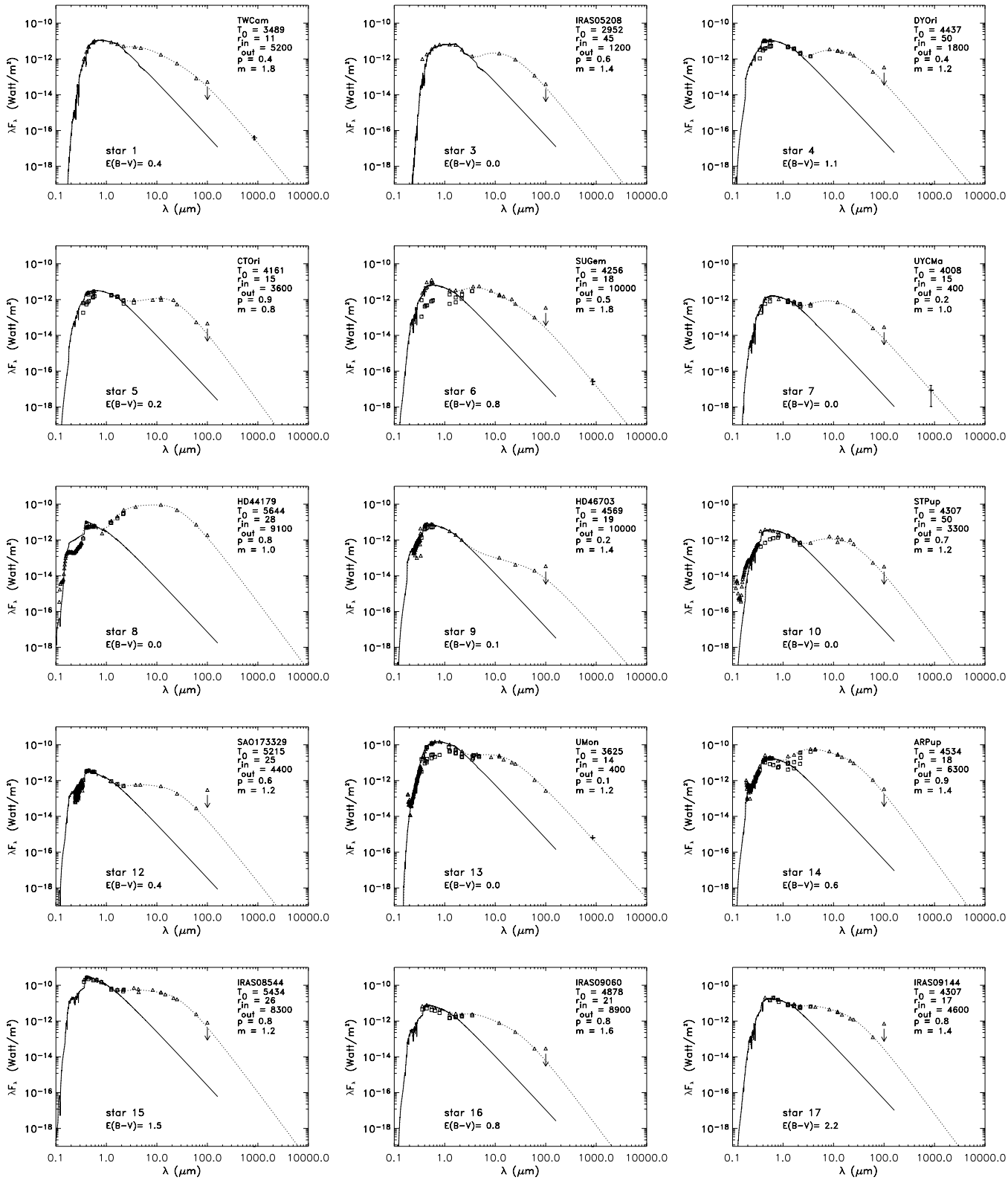

Fig. A.1. The SEDs of all post-AGB stars in our sample for which we have all the data needed to complete the SEDs, except those of HD 52961, HD 213985, RV Tau, IW Car, IRAS 17233 and IRAS 18123 (see Fig. 2). The dereddened fluxes are given together with the scaled photospheric Kurucz model representing the unattenuated stellar photosphere (solid line). An optically thin dust model was used to fit the IR excess (dotted line). Data found in the literature together with our 7 band Geneva photometry (only the maxima) are plotted as triangles. The minimal data points (squares) were not used for the determination of $E(B-V)$. They are shown to give an indication of the amplitude of the pulsations. Where available, crosses represent our 850 μm SCUBA data point. Error bars on the 850 μm SCUBA data point are plotted as well, for some objects though smaller than the symbols. The arrow at the 100 μm flux point signifies an upper limit.

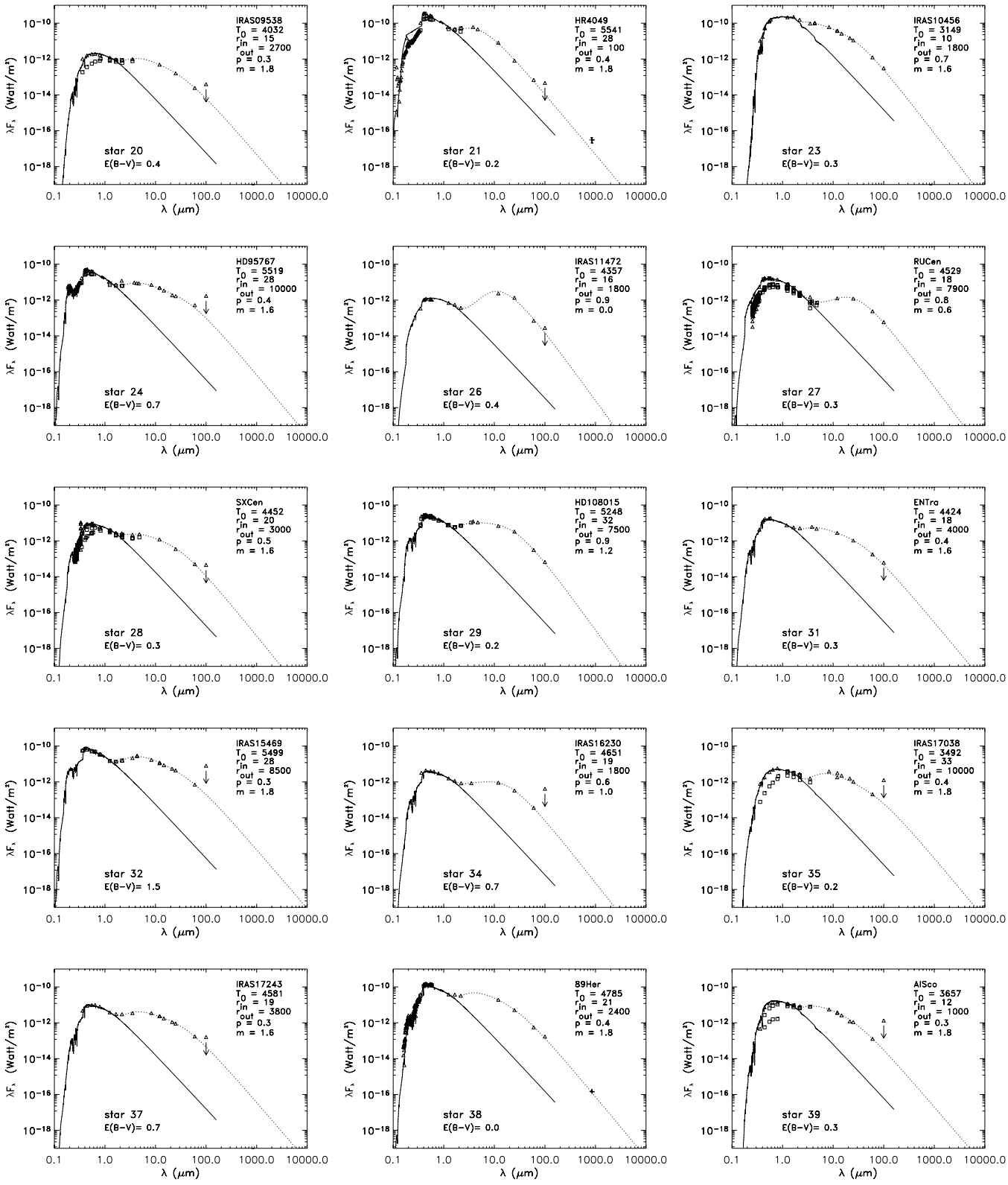

Fig. A.1. continued.

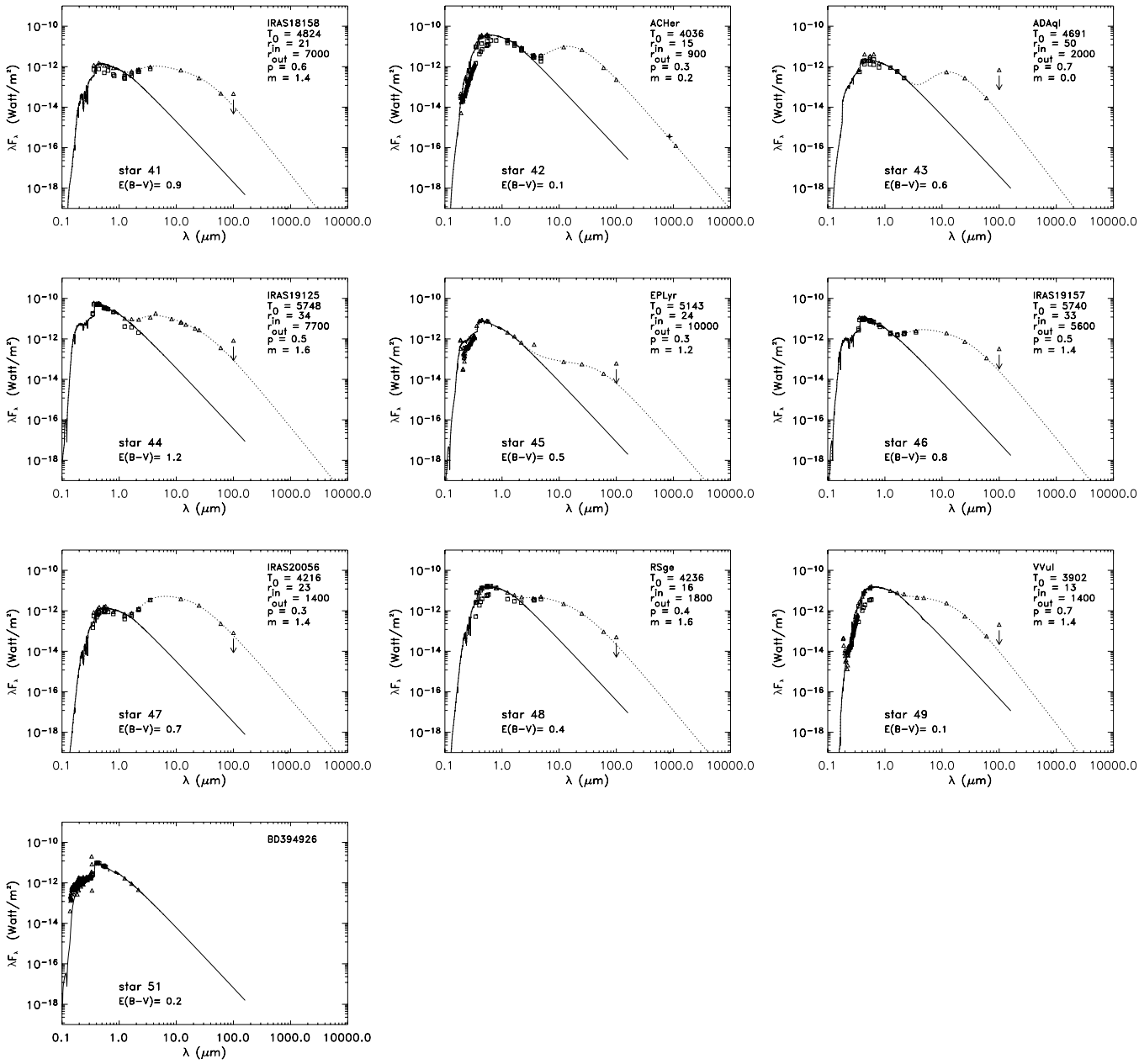

Fig. A.1. continued.

Appendix B: Orbital periods

Table B.1. The orbital period is given. Note that we included further refinements of our own based on longer time series. The original reference is given.

No	Name	$P_{\rm orbit}$ (days)	$a \sin i$ AU	Reference
8	HD 44179	319 ± 2	0.34	Van Winckel et al. (1995)
9	HD 46703	600 ± 2	0.92	Waelkens & Waters (1993)
10	ST Pup	410.4 ± 2.9	0.65	Gonzalez & Wallerstein (1996)
11	HD 52961	1310 ± 8	1.60	Van Winckel et al. (1999)
12	SAO 173329	115.9 ± 1	0.14	Van Winckel et al. (2000)
13	U Mon	±2597	3.6	Pollard & Cottrell (1995)
15	IRAS 08544	503 ± 2	0.38	Maas et al. (2003)
21	HR 4049	430.7 ± 1	0.60	Waelkens et al. (1991b)
24	HD 95767	±2050		Van Winckel et al. (2000)
28	SX Cen	595 ± 7	1.12	Maas et al. (2002)
31	EN TrA	1534 ± 21	2.07	Van Winckel et al. (1999)
38	89 Her	288.4 ± 4	0.08	Arellano Ferro (1984)
42	AC Her	1194 ± 6	1.39	Van Winckel et al. (1998)
50	HD 213985	259 ± 1	0.78	Van Winckel et al. (2000)
51	BD+39°4926	775 ± 5	0.10	Kodaira et al. (1970)

Appendix C: Data

Table C.1. Geneva data were acquired with the 70 cm Swiss Telescope at La Silla (Chile) and with the Flemish Mercator Telescope at La Palma (Spain), using the refurbished Geneva photometer P7 (Raskin et al. 2004). Our total dataset was scanned for the maximum and minimum magnitudes. Observation dates, number of measurements and total timebases of these maxima and minima are given as well. Additional data were found in the Geneva database: the General Catalogue of Photometric Data (GCPD, `http://obswww.unige.ch/gcpd/gcpd.html`).

No	Name	JD 2400000	Number	Timebase (days)	*U*	*B*	*V*	*B*1	*B*2	*V*1	*G*	Reference
1	TW Cam	52580.598	11	375	12.907	10.288	9.490	11.637	11.424	10.305	10.360	Mercator
		52295.400			13.000	10.499	9.716	11.807	11.642	10.533	10.579	Mercator
2	RV Tau	52305.412	37	827	12.511	9.957	9.036	11.323	11.077	9.859	9.886	Mercator
		52609.487			14.867	12.091	10.822	13.507	13.130	11.650	11.655	Mercator
4	DY Ori	52229.717	27	880	14.242	11.709	11.229	12.781	13.019	12.035	12.119	Mercator
		52986.649			15.447	12.933	12.078	14.177	14.167	12.908	12.921	Mercator
5	CT Ori	53021.482	31	884	12.119	10.020	10.174	10.993	11.397	10.924	11.175	Mercator
		52247.539			13.454	11.368	10.983	12.548	12.637	11.776	11.914	Mercator
6	SU Gem	52543.715	18	781	14.301	11.616	10.697	12.902	12.808	11.539	11.540	Mercator
		52307.508			16.610	14.028	13.248	15.160	15.386	14.042	14.057	Mercator
8	HD 44179				10.465	8.362	8.832	9.285	9.806	9.578	9.861	GCPD
		50403.809	96	2230	10.398	8.307	8.777	9.234	9.751	9.518	9.815	70 cm Swiss
		48705.546			10.565	8.470	8.938	9.390	9.921	9.684	9.972	70 cm Swiss
9	HD 46703				10.588	8.668	9.022	9.633	10.064	9.742	10.083	GCPD
		50100.497	104	6347	10.402	8.398	8.855	9.340	9.812	9.574	9.927	70 cm Swiss
		49300.642			10.889	8.998	9.251	9.995	10.361	9.989	10.309	70 cm Swiss
11	HD 52961				8.818	6.914	7.376	7.845	8.348	8.105	8.453	GCPD
		48575.657	177	5631	8.667	6.717	7.237	7.637	8.161	7.959	8.326	70 cm Swiss
		52612.675			8.955	7.080	7.522	8.013	8.504	8.253	8.592	Mercator
12	SAO 173329				12.420	10.320	10.642	11.297	11.721	11.382	11.687	GCPD
		47894.684	75	2917	12.392	10.290	10.609	11.256	11.674	11.352	11.653	70 cm Swiss
		49846.473			12.425	10.377	10.690	11.339	11.759	11.427	11.716	70 cm Swiss
13	U Mon				8.428	6.330	5.980	7.596	7.508	6.752	6.948	GCPD
		47545.766	110	1217	7.759	5.792	5.575	7.013	6.990	6.334	6.570	70 cm Swiss
		47853.822			9.507	7.484	7.194	8.697	8.698	7.941	8.245	70 cm Swiss
14	AR Pup				11.415	9.274	9.226	10.360	10.568	9.988	10.207	GCPD
		43605.517	2	416	11.313	9.229	9.179	10.318	10.511	9.935	10.165	70 cm Swiss
		43189.707			11.889	9.603	9.353	10.772	10.822	10.125	10.300	70 cm Swiss
21	HR 4049				7.010	4.896	5.504	5.808	6.349	6.221	6.617	GCPD
		45271.870	371	6943	6.570	4.584	5.284	5.471	6.056	5.997	6.421	70 cm Swiss
		47233.683			7.605	5.373	5.827	6.317	6.791	6.550	6.918	70 cm Swiss
23	IRAS 10456				10.460	7.480	6.292	9.144	8.455	7.130	7.117	GCPD
24	HD 95767				10.865	8.722	8.782	9.779	10.048	9.542	9.767	GCPD
		49086.620	102	6148	10.707	8.576	8.706	9.601	9.921	9.461	9.708	70 cm Swiss
		47636.567			10.941	8.816	8.840	9.887	10.125	9.596	9.808	70 cm Swiss
26	IRAS 11472	53548.427	1		13.645	11.619	11.790	12.622	12.949	12.533	12.824	Mercator
27	RU Cen				10.766	8.950	9.007	10.000	10.276	9.761	10.017	GCPD
		44778.506	23	751	10.219	8.429	8.574	9.441	9.773	9.320	9.591	70 cm Swiss
		44304.731			12.135	9.953	9.567	11.184	11.150	10.353	10.538	70 cm Swiss
28	SX Cen				11.732	9.735	9.636	10.858	11.005	10.400	10.616	GCPD
		44778.526	15	751	11.099	9.101	9.190	10.183	10.406	9.943	10.203	70 cm Swiss
		44669.855			12.912	10.907	10.545	12.109	12.132	11.329	11.472	70 cm Swiss
29	HD 108015				9.433	7.479	7.934	8.471	8.864	8.667	9.006	GCPD
		49386.836	111	2867	9.337	7.378	7.865	8.356	8.772	8.592	8.937	70 cm Swiss
		50115.801			9.541	7.606	8.020	8.613	8.975	8.749	9.082	70 cm Swiss
31	EN TrA				10.687	8.648	8.677	9.754	9.932	9.435	9.671	GCPD
		47636.730	61	2245	10.478	8.449	8.477	9.565	9.728	9.229	9.470	70 cm Swiss
		48133.582			11.293	9.181	9.088	10.350	10.439	9.852	10.056	70 cm Swiss
38	89 Her				6.860	4.869	5.425	5.815	6.296	6.148	6.526	GCPD
		41401.613	14	3507	6.769	4.779	5.364	5.714	6.212	6.080	6.471	70 cm Swiss
		41434.593			6.987	5.006	5.513	5.965	6.419	6.241	6.609	70 cm Swiss
40	IRAS 18123	52415.660	31	441	14.010	10.882	9.945	12.385	11.927	10.764	10.805	Mercator
		52508.430			14.719	11.420	10.267	13.023	12.428	11.090	11.119	Mercator

Table C.1. continued.

No	Name	JD 2400000	Number	Timebase (days)	U	B	V	$B1$	$B2$	$V1$	G	Reference
42	AC Her				9.419	7.450	7.456	8.536	8.755	8.221	8.460	GCPD
		52367.729	46	5038	8.726	6.900	7.261	7.854	8.311	8.002	8.310	Mercator
		52097.548			10.770	8.729	8.408	9.927	9.941	9.187	9.354	Mercator
43	AD Aql	52112.508	1		13.780	11.789	11.697	12.853	13.092	12.460	12.672	Mercator
44	IRAS 19125	52476.526	33	441	12.822	10.395	10.214	11.425	11.707	11.003	11.181	Mercator
		52428.678			12.875	10.466	10.289	11.516	11.784	11.064	11.237	Mercator
45	EP Lyr	52491.424	35	481	11.808	9.818	9.954	10.806	11.181	10.707	10.974	Mercator
		52136.422			13.144	11.134	10.880	12.267	12.371	11.648	11.841	Mercator
46	IRAS 19157	52561.390	4	60	12.968	10.690	10.688	11.694	12.058	11.468	11.659	Mercator
		52505.446			13.163	10.831	10.775	11.857	12.177	11.547	11.752	Mercator
47	IRAS 20056	52580.350	33	444	14.999	12.594	12.196	13.828	13.764	12.985	13.111	Mercator
		52854.611			15.429	12.943	12.505	14.213	14.122	13.274	13.392	Mercator
48	R Sge	52089.601	41	1164	11.471	9.183	8.925	10.413	10.376	9.700	9.869	Mercator
		52428.658			13.199	10.603	9.994	11.965	11.685	10.777	10.903	Mercator
49	V Vul	52131.599	39	1167	10.603	8.449	8.128	9.702	9.632	8.909	9.076	Mercator
		52419.684			12.555	10.187	9.728	11.454	11.350	10.494	10.740	Mercator
50	HD 213985				9.975	8.053	8.827	8.940	9.536	9.536	9.968	GCPD
		47397.749	156	5871	9.789	7.904	8.706	8.781	9.395	9.420	9.853	70 cm Swiss
		50051.540			10.618	8.556	9.209	9.478	10.008	9.922	10.327	70 cm Swiss
51	BD+39°4926				10.536	8.512	9.263	9.386	10.009	9.975	10.399	GCPD
		53250.653	70	14211	10.481	8.507	9.241	9.380	9.996	9.952	10.364	Mercator
		52561.442			10.502	8.528	9.278	9.408	10.026	9.979	10.407	Mercator

Table C.2. Ground-based optical (*UBVRI*) data, acquired over a long period, found in the literature. If possible the maximum and minimum magnitudes of a dataset are taken into account.

No	Name	JD 2400000	*U*	*B*	*V*	*R*	*I*	System	Reference
1	TW Cam		12.12	10.94	9.51			Johnson	Dawson (1979)
2	RV Tau		12.52	10.93	9.19			Johnson	Dawson (1979)
3	IRAS 05208	52294.367	11.132	10.498	9.352	8.643	7.947	Cousins	SAAO
		52253.552	11.185	10.665	9.608	8.915	8.139	Cousins	SAAO
4	DY Ori		13.45	12.75	11.48			Johnson	Dawson (1979)
5	CT Ori		11.69	11.24	10.31			Johnson	Dawson (1979)
6	SU Gem		12.88	11.70	10.19			Johnson	Dawson (1979)
7	UY CMa		11.36	11.03	10.40			Johnson	Dawson (1979)
			12.28	11.81	11.00			Johnson	Dawson (1979)
10	ST Pup	48363.260	9.890	9.686	9.362	9.126	8.835	Cousins	Kilkenny et al. (1993)
		48672.365	12.058	11.568	10.661	10.151	9.642	Cousins	Kilkenny et al. (1993)
13	U Mon		7.15	6.59	5.66			Johnson	Dawson (1979)
		49258.126		6.497	5.436	4.946	4.511	Cousins	Pollard et al. (1996)
		48499.199		8.614	7.632	7.088	6.387	Cousins	Pollard et al. (1996)
14	AR Pup	48622.972		9.782	9.093	8.672	8.216	Cousins	Pollard et al. (1996)
		48854.238		10.823	10.092	9.638	9.186	Cousins	Pollard et al. (1996)
15	IRAS 08544	51609.372	11.660	10.533	9.017	8.052	7.024	Cousins	SAAO
		51300.233	11.982	10.756	9.192	8.186	7.139	Cousins	SAAO
16	IRAS 09060	50957.232	12.390	11.817	10.959	10.383	9.749	Cousins	SAAO
		49399.455	12.893	12.305	11.417	10.839	10.227	Cousins	SAAO
17	IRAS 09144	51625.329			13.857	12.267	10.777	Cousins	SAAO
		51626.333		15.886	13.890	12.293	10.797	Cousins	SAAO
18	IW Car	48650.035		8.657	7.852	7.379	6.772	Cousins	Pollard et al. (1996)
		48911.056		9.755	8.758	8.148	7.454	Cousins	Pollard et al. (1996)
20	IRAS 09538	52030.329	12.772	12.083	11.161	10.623	10.056	Cousins	SAAO
		51576.506	14.638	13.733	12.485	11.691	10.901	Cousins	SAAO
23	IRAS 10456	49053.470	9.829	7.942	6.246			Cousins	SAAO
		49078.387	9.869	7.963	6.267			Cousins	SAAO
27	RU Cen	46244.28	11.31	10.46	9.43	8.89	8.38	Cousins	Goldsmith et al. (1987)
		46245.34	11.44	10.59	9.53	8.98	8.47	Cousins	Goldsmith et al. (1987)
		48269.101		9.158	8.529	8.178	7.606	Cousins	Pollard et al. (1996)
		48319.041		10.798	9.811	9.294	8.688	Cousins	Pollard et al. (1996)
28	SX Cen	46243.26	10.85	10.26	9.43	8.97	8.53	Cousins	Goldsmith et al. (1987)
		46248.30	11.36	10.70	9.77	9.27	8.81	Cousins	Goldsmith et al. (1987)
29	HD 108015	52734.477	8.524	8.225	7.834	7.598	7.343	Cousins	SAAO
		53139.350	8.873	8.506	8.048	7.771	7.498	Cousins	SAAO
32	IRAS 15469	49489.459	12.985	11.921	10.493	9.609	8.676	Cousins	SAAO
		49442.626	13.063	12.090	10.622	9.718	8.769	Cousins	SAAO
34	IRAS 16230	49585.254	12.800	12.102	11.157	10.585	9.985	Cousins	SAAO
		53129.518	13.324	12.760	11.628	10.915	10.272	Cousins	SAAO
35	IRAS 17038	52411.554	12.229	11.241	9.922	9.158	8.420	Cousins	SAAO
		51786.255	14.756	13.453	11.916	10.982	9.895	Cousins	SAAO
36	IRAS 17233	51663.588	12.719	12.312	11.705	11.287	10.830	Cousins	SAAO
		49590.265	14.219	13.564	12.663	12.172	11.722	Cousins	SAAO
37	IRAS 17243	52837.410	12.378	11.316	10.200	9.544	8.919	Cousins	SAAO
		52507.388	13.479	12.216	10.915	10.186	9.507	Cousins	SAAO
39	AI Sco	46245.48	13.21	11.16	9.55	8.73	7.92	Cousins	Goldsmith et al. (1987)
		49238.995		10.088	8.868	8.215	7.656	Cousins	Pollard et al. (1996)
		4823.095		12.884	11.422	10.623	9.954	Cousins	Pollard et al. (1996)
40	IRAS 18123	49537.405	13.033	11.335	9.876	9.146	8.524	Cousins	SAAO
		49970.295	13.907	12.062	10.537	9.781	9.030	Cousins	SAAO

Table C.2. continued.

No	Name	JD 2400000	*U*	*B*	*V*	*R*	*I*	System	Reference
41	IRAS 18158	48799.539	14.720	13.970	13.070	12.380	11.670	Cousins	SAAO
		49172.542	14.857	14.349	13.699	12.742	12.312	Cousins	SAAO
42	AC Her		8.00	7.66	7.03			Johnson	Dawson (1979)
		46248.47	9.11	8.68	7.87	7.40	6.91	Cousins	Goldsmith et al. (1987)
43	AD Aql	46253.53	14.30	12.61	11.07	10.26		Cousins	Goldsmith et al. (1987)
		48524.899		11.811	11.285	10.917	10.534	Cousins	Pollard et al. (1996)
		48152.985		13.039	12.097	11.558	11.069	Cousins	Pollard et al. (1996)
44	IRAS 19125	49563.415	11.724	11.097	10.100	9.438	8.661	Cousins	SAAO
		49510.555	11.921	11.237	10.215	9.532	8.731	Cousins	SAAO
45	EP Lyr		10.92	10.69	10.12			Johnson	Dawson (1979)
46	IRAS 19157	49207.444	11.862	11.398	10.624	10.126	9.588	Cousins	SAAO
		51761.419	12.160	11.605	10.753	10.213	9.632	Cousins	SAAO
47	IRAS 20056	46654.41	14.25	13.44	12.37	11.79	11.29	Cousins	Menzies & Whitelock (1988)
		46627.46	14.31	13.61	12.55	11.94	11.39	Cousins	Menzies & Whitelock (1988)
48	R Sge		11.04	9.93	8.84			Johnson	Dawson (1979)
		46242.57	10.43	9.71	8.79	8.31	7.84	Cousins	Goldsmith et al. (1987)
		46243.58	10.57	9.79	8.83	8.32	7.84	Cousins	Goldsmith et al. (1987)
49	V Vul		9.70	9.09	8.27			Johnson	Dawson (1979)

Table C.3. Ground-based near-infrared (*JHKLM*) photometry found in the literature. If there was more than one measurement we used both the maximum and minimum datapoints. For the data from 2 MASS and DENIS we made use of the catalogues found in VIZIER (`http://vizier.u-strasbg.fr/viz-bin/VizieR`).

No	Name	JD 2400000	*I*	*J*	*H*	*K*	*L*	*M*	System	Reference
1	TW Cam						4.2	3.5	Mt Lemmon Arizona system	Gehrz (1972)
		42445.45		7.04	6.36	5.70	4.40		Tenerife	Lloyd Evans (1985)
				7.035	6.364	5.750			2 MASS	VIZIER
2	RV Tau					5.1	3.3	2.3	Mt Lemmon Arizona system	Gehrz (1972)
		42445.48		6.39	5.67	5.03	3.64		Tenerife	Lloyd Evans (1985)
				6.183	5.488	4.777			2 MASS	VIZIER
3	IRAS 05208	48637.35		7.05	6.24	6.05	5.64		SAAO	T. Lloyd Evans
		49313.47		7.20	6.38	6.13	5.64		SAAO	T. Lloyd Evans
			8.705	6.408		5.953			DENIS	VIZIER
				7.044	6.314	6.063			2 MASS	VIZIER
4	DY Ori	43189.30		8.10	7.47	7.02	5.73		SAAO	Lloyd Evans (1985)
		43158.44		8.30	7.40	6.90	5.80		SAAO	Lloyd Evans (1985)
				8.073	7.381	6.983			2 MASS	VIZIER
5	CT Ori	43184.37		8.57	7.82	8.00	6.48		SAAO	Lloyd Evans (1985)
		43158.38		8.66	7.92	7.50	6.09		SAAO	Lloyd Evans (1985)
				8.404	7.931	7.607			2 MASS	VIZIER
6	SU Gem						4.1	3.2	Mt Lemmon Arizona system	Gehrz (1972)
		43160.37		8.36	7.38	6.47	4.94		SAAO	Lloyd Evans (1985)
		43188.32		8.97	8.38	6.95	4.96		SAAO	Lloyd Evans (1985)
				10.167	9.033	7.584			2 MASS	VIZIER
7	UY CMa	46107.32		9.35	8.82	8.22	6.62		SAAO	Lloyd Evans (1985)
		43159.36		9.42	8.46	8.41	6.87		SAAO	Lloyd Evans (1985)
			9.845	9.093		8.038			DENIS	VIZIER
				9.042	8.597	7.986			2 MASS	VIZIER
8	HD 44179			6.59	4.95	3.19	1.22		ESO	C. Waelkens
			8.981	6.280		3.807			DENIS	VIZIER
				6.577	5.145	3.655			2 MASS	VIZIER
9	HD 46703			7.805	7.513	7.435			2MASS	VIZIER
10	ST Pup	43159.44		8.38	8.03	7.67	6.42		SAAO	Lloyd Evans (1985)
			9.292	8.437		7.839			DENIS	VIZIER
				8.506	8.250	8.082			2 MASS	VIZIER
11	HD 52961			6.36	5.98	5.54	4.25	3.97	ESO	C. Waelkens
				6.323	5.978	5.526			2 MASS	VIZIER
12	SAO 173329			9.42	8.96	8.27	6.49	5.67	ESO	C. Waelkens
				9.375	8.917	8.308			2 MASS	VIZIER
13	U Mon						2.4	1.5	Kitt Peak NO Arizona system	Gehrz & Woolf (1970)
						3.7	2.7	1.7	Mt Lemmon Arizona system	Gehrz (1972)
		42684.65		4.01	3.65	3.25	2.40		SAAO	Lloyd Evans (1985)
		43160.45		4.88	4.43	4.08	3.08		SAAO	Lloyd Evans (1985)
				4.35	3.93	3.60	2.30	1.61	ESO	C. Waelkens
				4.925	4.269	4.042			2 MASS	VIZIER
14	AR Pup	43184.46		6.12	4.95	3.67	1.68		SAAO	Lloyd Evans (1985)
		42737.58		7.20	5.98	4.40	2.08		SAAO	Lloyd Evans (1985)
			8.937	6.931		3.682			DENIS	VIZIER
				7.891	6.824	5.285			2 MASS	VIZIER
15	IRAS 08544			5.65	4.67	3.51	1.59		SAAO	T. Lloyd Evans (mean)
			9.043	5.741		3.813			DENIS	VIZIER
				5.575	4.743	3.523			2 MASS	VIZIER

Table C.3. continued.

No	Name	JD 2400000	*I*	*J*	*H*	*K*	*L*	*M*	System	Reference
16	IRAS 09060	50263.20		8.60	7.63	6.68	5.16		SAAO	T. Lloyd Evans
		50511.38		9.27	8.13	6.99	5.35		SAAO	T. Lloyd Evans
				9.130	8.060	6.949			2 MASS	VIZIER
17	IRAS 09144	49125.31		8.33	7.12	6.00	4.23		SAAO	T. Lloyd Evans
		49475.28		8.55	7.35	6.21	4.31		SAAO	T. Lloyd Evans
			10.801	8.305		6.235			DENIS	VIZIER
				8.372	7.391	6.369			2 MASS	VIZIER
18	IW Car	43184.48		5.86	5.18	4.24	2.41		SAAO	Lloyd Evans (1985)
		43155.56		5.94	5.20	4.31	2.44		SAAO	Lloyd Evans (1985)
				5.875	5.151	4.367			2 MASS	VIZIER
19	IRAS 09400	49122.29		6.57	5.58	5.16	4.33		SAAO	T. Lloyd Evans
		50511.40		6.61	5.59	5.20	4.35		SAAO	T. Lloyd Evans
				6.547	5.626	5.159			2 MASS	VIZIER
20	IRAS 09538	49741.57		9.18	8.49	7.61	6.09		SAAO	T. Lloyd Evans
		49031.52		9.62	8.82	8.02	6.36		SAAO	T. Lloyd Evans
			10.530	9.278		7.703			DENIS	VIZIER
				9.402	8.574	7.721			2 MASS	VIZIER
21	HR 4049			4.73	4.16	3.13	1.39	0.91	ESO	C. Waelkens
						3.677			DENIS	VIZIER
				4.921	4.225	3.208			2 MASS	VIZIER
22	IRAS 10174	49474.35		5.20	4.07	3.54	2.87		SAAO	T. Lloyd Evans
		50262.22		5.43	4.29	3.74	3.04		SAAO	T. Lloyd Evans
			8.644	5.583		3.481			DENIS	VIZIER
				5.313	4.490	3.931			2 MASS	VIZIER
23	IRAS 10456			3.45	2.55	2.15	1.11		SAAO	T. Lloyd Evans (mean)
				3.354	2.469	2.045			2 MASS	VIZIER
24	HD 95767			7.05	6.48	5.59	3.50	2.80	ESO	C. Waelkens
			8.786	7.313		4.964			DENIS	VIZIER
				7.098	6.532	5.636			2 MASS	VIZIER
25	GK Car	43184.56		9.05	8.26	8.14	6.42		SAAO	Lloyd Evans (1985)
		43159.52		9.27	8.46	7.87	6.64		SAAO	Lloyd Evans (1985)
			10.150	9.123		7.970			DENIS	VIZIER
				9.328	8.716	8.171			2 MASS	VIZIER
26	IRAS 11472			9.657	9.047	8.630			2 MASS	VIZIER
27	RU Cen	43188.51		7.08	6.65	6.47	6.53		SAAO	Lloyd Evans (1985)
		43158.58		7.14	6.68	6.39	5.63		SAAO	Lloyd Evans (1985)
		46243.25		7.56	7.04	6.83	6.33	5.60	SAAO	Goldsmith et al. (1987)
		46248.28		8.00	7.44	7.20			SAAO	Goldsmith et al. (1987)
				7.45	7.02	6.73	6.08	5.47	ESO	C. Waelkens
				7.68	7.15	6.86	6.34	5.80	ESO	Garcia-Lario et al. (1997)
			8.600	7.151		6.654			DENIS	VIZIER
				7.616	7.186	6.918			2 MASS	VIZIER
28	SX Cen	43159.57		7.94	7.63	6.88	5.74		SAAO	Lloyd Evans (1985)
		46243.26		7.86	7.25	6.62	5.20	4.30	SAAO	Goldsmith et al. (1987)
		46248.30		8.12	7.51	7.00	5.65	4.73	SAAO	Goldsmith et al. (1987)
			8.962	7.660		6.448			DENIS	VIZIER
				7.875	7.443	6.759			2 MASS	VIZIER
29	HD 108015			7.03	6.39	5.32	3.50		SAAO	T. Lloyd Evans (mean)
				7.03	6.40	5.28	3.14	2.49	ESO	C. Waelkens
				6.941	6.380	5.338			2 MASS	VIZIER
30	IRAS 13258	50508.64		11.65	9.87	8.29	6.52		SAAO	T. Lloyd Evans
		50204.46		12.11	10.05	8.48	6.56		SAAO	T. Lloyd Evans
			14.474	12.569					DENIS	VIZIER
				12.160	10.630	9.303			2 MASS	VIZIER

Table C.3. continued.

No	Name	JD 2400000	*I*	*J*	*H*	*K*	*L*	*M*	System	Reference
31	EN TrA	42945.38		7.19	6.67	6.03	4.69		SAAO	Lloyd Evans (1985)
				7.10	6.53	5.73	3.92	3.38	ESO	C. Waelkens
				7.092	6.578	5.931			2 MASS	VIZIER
32	IRAS 15469			7.24	6.21	4.89	2.89		SAAO	T. Lloyd Evans (mean)
				7.190	6.235	4.967			2 MASS	VIZIER
33	IRAS 15556	48778.44		9.42	8.34	6.89	4.55		SAAO	T. Lloyd Evans
		50642.32		9.51	8.38	6.88	4.49		SAAO	T. Lloyd Evans
			10.877	9.440		6.887			DENIS	VIZIER
				9.423	8.350	6.940			2 MASS	VIZIER
34	IRAS 16230	49124.51		9.10	8.48	7.79	6.29		SAAO	T. Lloyd Evans
		48819.36		9.37	8.77	8.12	6.26		SAAO	T. Lloyd Evans
				9.002	8.510	7.812			2 MASS	VIZIER
35	IRAS 17038	50641.37		7.74	7.00	6.58	5.54		SAAO	T. Lloyd Evans
		49473.66		8.36	7.64	7.16	6.11		SAAO	T. Lloyd Evans
			9.434	7.791		6.369			DENIS	VIZIER
				7.622	7.050	6.523			2 MASS	VIZIER
36	IRAS 17233	50204.56		10.03	8.89	7.28	4.86		SAAO	T. Lloyd Evans
		49474.60		10.89	9.68	7.72	5.09		SAAO	T. Lloyd Evans
				10.423	9.592	8.371			2 MASS	VIZIER
37	IRAS 17243			8.17	7.46	6.52	4.75		SAAO	T. Lloyd Evans (mean)
			9.314	8.177		6.592			DENIS	VIZIER
				8.035	7.358	6.462			2 MASS	VIZIER
38	89 Her			4.998	4.239	3.632			2 MASS	VIZIER
39	AI Sco	42997.35		6.74	5.94	5.14	3.79		SAAO	Lloyd Evans (1985)
		46245.48		6.62	5.98	5.33	3.81		SAAO	Goldsmith et al. (1987)
				6.864	6.179	5.485			2 MASS	VIZIER
40	IRAS 18123			8.04	7.44	6.86	5.39		SAAO	T. Lloyd Evans (mean)
				7.974	7.399	6.729			2 MASS	VIZIER
41	IRAS 18158	48778.52		10.52	9.31	8.01	6.40		SAAO	T. Lloyd Evans
		50204.60		11.15	9.80	8.27	6.17		SAAO	T. Lloyd Evans
			12.341	10.958		8.291			DENIS	VIZIER
				10.788	9.489	8.120			2 MASS	VIZIER
42	AC Her						4.4	4.0	Kitt Peak NO Arizona system	Gehrz & Woolf (1970)
						5.2	4.7	3.6	Mt Lemmon Arizona system	Gehrz (1972)
		42456.87		5.97	5.52	5.28	4.73		Tenerife	Lloyd Evans (1985)
		46243.52		5.89	5.39	5.16	4.66	3.90	SAAO	Goldsmith et al. (1987)
		46248.47		6.21	5.66	5.40	4.87	4.55	SAAO	Goldsmith et al. (1987)
				5.700	5.338	5.075			2 MASS	VIZIER
43	AD Aql	46253.53		9.62	9.14	8.95			SAAO	Goldsmith et al. (1987)
				9.543	9.134	9.002			2 MASS	VIZIER
44	IRAS 19125			7.48	6.47	5.38	3.52		SAAO	T. Lloyd Evans (mean)
				8.356	7.442	7.067			2 MASS	VIZIER
45	EP Lyr						6.6		Mt Lemmon Arizona system	Gehrz (1972)
				8.534	8.153	8.030			2 MASS	VIZIER

Table C.3. continued.

No	Name	JD 2400000	*I*	*J*	*H*	*K*	*L*	*M*	System	Reference
46	IRAS 19157	48779.58		8.89	8.12	6.95	5.13		SAAO	T. Lloyd Evans
		48820.44		8.94	8.16	6.92	5.32		SAAO	T. Lloyd Evans
			9.713	8.966		7.109			DENIS	VIZIER
				8.872	8.205	7.020			2 MASS	VIZIER
47	IRAS 20056	45897.49		9.99	8.89	7.31	4.77		SAAO	Menzies & Whitelock (1988)
		46693.29		10.55	9.20	7.43	4.78		SAAO	Menzies & Whitelock (1988)
				10.097	8.964	7.471			2 MASS	VIZIER
48	R Sge						4.5	3.3	Kitt Peak NO Arizona system	Gehrz & Woolf (1970)
							4.6	3.6	Mt Lemmon Arizona system	Gehrz (1972)
		46248.54		7.10	6.50	5.80	4.50		SAAO	Goldsmith et al. (1987)
				7.818	7.234	6.539			2 MASS	VIZIER
49	V Vul						4.2	3.4	Mt Lemmon Arizona system	Gehrz (1972)
				6.557	6.019	5.396			2 MASS	VIZIER
50	HD 213985			8.18	7.60	6.68	5.00	4.45	ESO	C. Waelkens
				8.276	7.609	6.705			2 MASS	VIZIER
51	BD+39°4926			8.539	8.394	8.338			2 MASS	VIZIER

Table C.4. IRAS photometry points at 12, 25, 60 and 100 μm. Note however that in some cases the data points are upper limits (L); these observations are probably contaminated by interstellar cirrus clouds. Other data are lower limits (:). Remark also that for BD+39°4926 we don't have IRAS datapoints.

No	Name	F_{12} (Jy) 12 μm	F_{25} (Jy) 25 μm	F_{60} (Jy) 60 μm	F_{100} (Jy) 100 μm
1	TW Cam	8.25	5.60	1.84	1.79L
2	RV Tau	22.52	18.05	6.50	2.44:
3	IRAS 05208	9.53	9.30	2.78	1.40
4	DY Ori	12.43	14.89	4.18	11.46L
5	CT Ori	6.14	5.55	1.24	1.59L
6	SU Gem	7.91	5.68	2.19	11.99L
7	UY CMa	3.49	2.46	0.57	1.00L
8	HD 44179	421.60	456.10	173.10	66.19
9	HD 46703	0.46	0.38:	0.40L	1.15L
10	ST Pup	3.51	5.92	1.24	1.13L
11	HD 52961	4.53	2.22	0.95	0.87:
12	SAO 173329	2.28	1.83	0.64	10.45L
13	U Mon	124.30	88.43	26.59	9.54
14	AR Pup	131.30	94.32	26.12	11.96:
15	IRAS 08544	180.30	158.80	56.25:	28.43L
16	IRAS 09060	3.78	2.53	0.65	1.00L
17	IRAS 09144	15.31	12.14	2.86	24.68L
18	IW Car	101.00	96.24	34.52	13.46
19	IRAS 09400	7.85	5.48	1.58	8.34L
20	IRAS 09538	2.33	1.60	0.53	1.34L
21	HR 4049	48.25	9.55	1.77	1.69L
22	IRAS 10174	41.80	60.39	16.13:	174.30L
23	IRAS 10456	189.10	115.50	30.86	10.89
24	HD 95767	22.13	15.65	10.90	58.88
25	GK Car	2.85	2.45	0.79	12.41L
26	IRAS 11472	11.35	14.18	1.78	1.00L
27	RU Cen	5.32	10.96	5.65	2.09
28	SX Cen	5.92	3.59	1.10	1.55L
29	HD 108015	32.46	33.23	7.99	2.41
30	IRAS 13258	1.90	2.97	1.46	3.82:
31	EN TrA	13.20	10.30	4.11	2.12
32	IRAS 15469	48.81	42.12	15.50	278.10L
33	IRAS 15556	19.86	17.80	7.10	189.80L
34	IRAS 16230	4.29	3.34	0.82	14.55L
35	IRAS 17038	8.05	9.67	4.49	43.34L
36	IRAS 17233	17.02	13.40	3.67	32.08L
37	IRAS 17243	10.76	8.77	3.69	5.41:
38	89 Her	97.52	54.49	13.42	6.04
39	AI Sco	17.59	11.38	2.95	46.76L
40	IRAS 18123	10.72	11.02	4.21	1.85L
41	IRAS 18158	3.00	2.64	1.03	1.56L
42	AC Her	41.43	65.33	21.37	8.04
43	AD Aql	2.49	2.72	0.65L	24.46L
44	IRAS 19125	28.89	26.51	7.81	28.05L
45	EP Lyr	0.31L	0.50	0.40L	2.10L
46	IRAS 19157	8.88	7.16	2.45	11.05L
47	IRAS 20056	17.52	18.01	5.38	2.84L
48	R Sge	10.60	7.54	2.12	1.72L
49	V Vul	12.35	5.69	1.29	7.25L
50	HD 213985	5.57	4.66	2.11	1.01L

Table C.5. Data of the Midcourse Space eXperiment (MSX). The instrument on board MSX is the SPIRIT III (Spatial Infrared Imaging Telescope III). The approximate effective wavelengths of the 6 MSX filters are in μm.

No	Name	B1 (Jy) 4.29 μm	B2 (Jy) 4.35 μm	A (Jy) 8.28 μm	C (Jy) 12.13 μm	D (Jy) 14.65 μm	E (Jy) 21.34 μm
4	DY Ori			9.073	11.58	11.89	13.97
5	CT Ori			2.618	3.928	1.421	6.761
6	SU Gem			8.283	7.666	7.178	7.505
10	ST Pup			4.419	5.743	5.464	7.199
13	U Mon		42.93	56.45	88.71	72.38	73.29
14	AR Pup	72.73	81.04	114.3	118.0	100.2	91.48
15	IRAS 08544	76.62	51.92	139.0	150.7	143.6	134.2
17	IRAS 09144		7.285	10.69	11.61	10.31	9.341
19	IRAS 09400			4.814	3.847	3.072	3.034
22	IRAS 10174	16.89	19.14	25.84	33.91	28.70	45.77
23	IRAS 10456	139.5	147.8	165.4	148.1	126.7	106.3
24	HD 95767		12.33	18.96	18.70	16.33	13.09
25	GK Car			2.774	2.630	2.172	2.086
32	IRAS 15469	34.65	35.82	42.91	45.97	40.16	37.48
33	IRAS 15556			16.63	17.50	17.20	14.98
35	IRAS 17038			10.45	12.66	10.93	11.09
36	IRAS 17233			13.94	15.28	12.87	10.74
37	IRAS 17243			9.254	9.280	8.408	7.775
39	AI Sco			15.26	14.89	12.72	8.562
44	IRAS 19125		23.43	24.55	26.48	23.90	22.54

Table C.6. 850 μm fluxes from observations with the Submillimetre Common-User Bolometer Array (SCUBA) at the James Clerk Maxwell Telescope (JCMT), Mauna Kea, Hawaii.

No	Name	F_{850} (mJy)	Reference
1	TW Cam	11.0 ± 2.3	De Ruyter et al. (2005)
2	RV Tau	50.3 ± 3.6	De Ruyter et al. (2005)
6	SU Gem	7.5 ± 2.5	De Ruyter et al. (2005)
7	UY CMa	2.4 ± 2.1	De Ruyter et al. (2005)
11	HD 52961	2.8 ± 1.9	new data
13	U Mon	181.6 ± 2.6	De Ruyter et al. (2005)
21	HR 4049	8.7 ± 2.8	new data
		10.4 ± 2.2	Dominik et al. (2003)
38	89 Her	40.9 ± 2.4	new data
42	AC Her	99.4 ± 3.8	De Ruyter et al. (2005)
47	IRAS 20056	21.8 ± 1.8	Gledhill et al. (2002)